Politecnico di Torino

Politecnico di Torino

Mechatronics Engineering

A.a. 2025/2026

Sessione di laurea 03/2026

Investigation of Octopus Arm Tip Behaviour for Bio-Inspired Soft Robotic Arm Control

Relatori:

Stefano Paolo Pastorelli

Barbara Mazzolai

Candidata:

Agnese Favaro

Ringraziamenti

I would like to sincerely thank Barbara Mazzolai and Laura Margheri for giving me the opportunity to carry out this work at the Italian Institute of Technology. This experience has been extremely interesting and valuable for my academic and personal development.

I would also like to express my gratitude to Yasmin Tauqueer Ansari and Professor Stefano Paolo Pastorelli for their guidance, support, and supervision throughout this project.

Finally, I would like to thank the Aquarium of Genoa and all the biologists involved for the wonderful opportunity to conduct experimental observations in such a unique environment.

Indice

Elenco delle figure

Capitolo 1

Introduction

Traditional rigid-body robots have enabled the development of high-precision and high-repeatability automation systems, particularly effective in structured environments where tasks and operating conditions can be closely controlled. These systems typically rely on articulated kinematic chains consisting of discrete joints and a defined number of degrees of freedom, which allow precise description and control of the robot's movement. However, this rigid architecture also represents a significant limitation when robots need to operate in more complex contexts, such as interacting with fragile objects, performing tasks in unstructured or uncertain environments, or physically collaborating directly with humans. In such scenarios, careful motion planning is not sufficient: robots must be able to tolerate uncertainty, absorb impacts, and adapt their shape and contact conditions to the surrounding environment.

1.1 Soft robotics

These limitations have motivated the emergence of soft robotics, a research field inspired by the compliance and continuous deformation properties observed in biological organisms with soft bodies, particularly in muscular hydrostats (Fig. 1.1) [1, 2]. Soft robotics can be broadly defined as the design and creation of robotic systems whose bodies, or significant functional components, are made with highly deformable and compliant materials, often inspired by biological organisms [3]. The main goal of this field is to exploit the principles present in natural systems to develop robots capable of adapting to the environment, interacting safely with objects and people, and performing complex movements through distributed body deformations.

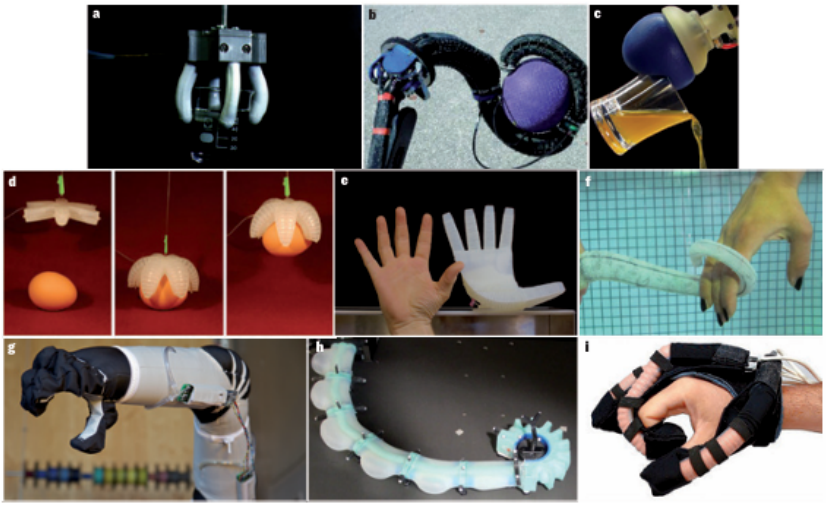

Figura 1.1: Representative examples of soft robotic systems illustrating the use of compliant materials and continuous deformation for adaptive locomotion, manipulation, and safe interaction: (a) microactuation [4], (b) soft-continuum manipulation [5], (c) particle jamming gripper [6], (d) soft lithography gripper fabrication [7], (e) underactuated dexterous grasping [8], (f) octopus-inspired manipulation [9], (g) inflatable robotic manipulator [10], (h) feedback control of a multisegmented arm [11], (i) soft rehabilitation glove [12].

Unlike rigid robots, in soft robots movement is not concentrated in discrete joints but is distributed throughout the entire structure of the system. This continuous deformation allows for large shape changes and a potentially high number of effective degrees of freedom. The intrinsic compliance of the materials used also improves safety during physical interaction and allows the robot to adapt to geometric variability and positioning errors in contact with the environment [1]. In this context, biological inspiration plays a central role: many soft robotics systems are designed by emulating the morphology and movement strategies of highly deformable organisms, such as tentacle appendages, peristaltic worms, or aquatic animals (Fig. 1.2).These biological models demonstrate how complex and adaptive movements can emerge from the interaction between materials, structure, and environment, rather than being entirely determined by control algorithms.

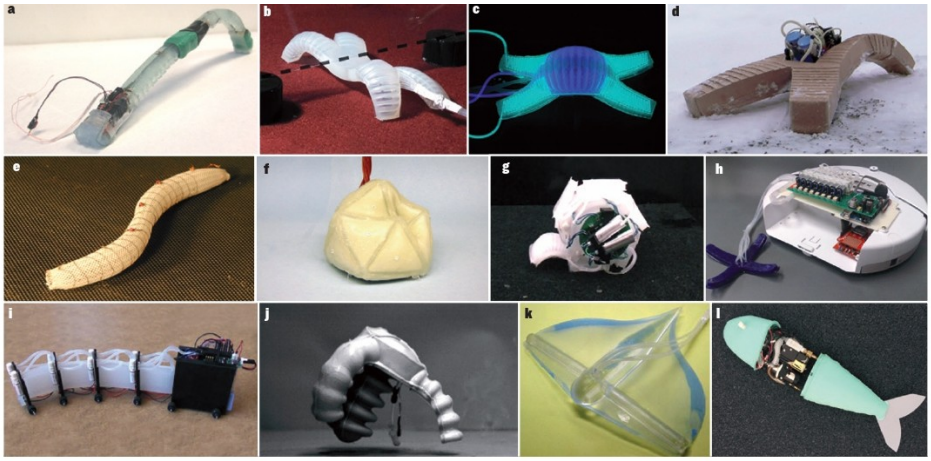

Figura 1.2: Examples of bio-inspired soft robotic systems demonstrating different locomotion strategies enabled by compliant materials and distributed deformation: (a) caterpillar-inspired locomotion [13], (b) multi-gait quadruped robot [14], (c) active camouflage robot [15], (d) walking in hazardous environments [16], (e) worm-inspired locomotion [17], (f) particle-jamming based actuation [18], (g) rolling robot powered by pneumatic actuation [19], (h) hybrid hard–soft robot [20], (i) snake-inspired locomotion [21], (j) jumping robot [22], (k) manta-ray inspired swimming robot [23], (l) autonomous fish [24]

1.1.1 Embodied Intelligence

This is the perspective of *embodied intelligence*, according to which material properties, geometry, and morphology directly contribute to system functionality. In soft robotic systems, intelligence is not exclusively encoded in control software, but is partially embedded in the physical structure of the robot itself, reducing the reliance on precise modeling and high-bandwidth control [25, 3]. This concept is strongly inspired by biological systems, in which body, control, and environment are tightly coupled and co-evolve to produce adaptive behavior [26].

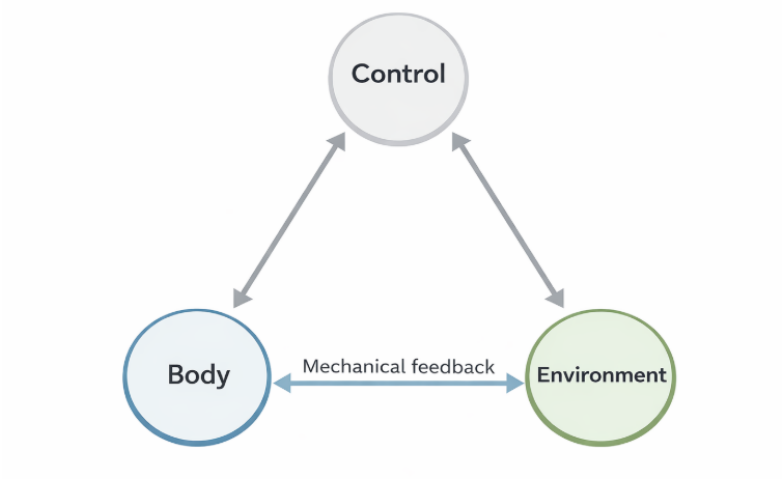

Figura 1.3: Conceptual representation of embodied intelligence, where system behavior emerges from the interaction between the physical body, the control system, and the environment. Mechanical feedback arising from body–environment interaction can directly influence the system response.

A more detailed interpretation of embodied intelligence in robotic systems is illustrated in Fig. 1.4, where sensing, actuation, control, and environmental interaction form a closed loop. In this framework, actuation inputs are not translated into motion through control alone, but are mediated by the mechanical properties of the compliant structure and by its interaction with the surrounding environment. As a result, the resulting behavior emerges from the physical coupling between actuation, body mechanics, and environmental forces, which allows part of the system behavior to emerge directly from the interaction between actuation, body mechanics, and the environment [27].

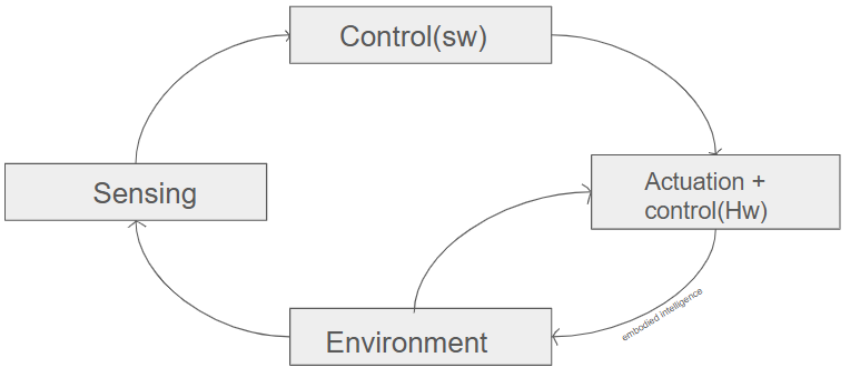

Figura 1.4: Extended representation of embodied intelligence in robotic systems. The diagram highlights the interaction between sensing, control software, actuation hardware, and the environment. In soft robots, actuation mechanisms interact with compliant structures and environmental forces to generate adaptive behavior.

1.1.2 Actuation Technologies

Overall, soft robotics should be regarded not merely as a collection of technologies, but as a design philosophy in which materials, morphology, and interaction play a central role. While a wide variety of actuation principles, fabrication techniques, and control strategies have been developed, they all share the common objective of exploiting compliance and continuous deformation to achieve safe, adaptive, and robust behavior. At the same time, the use of soft materials introduces open challenges in modeling, control, and sensing integration, which remain central research topics in the field [2, 28].

1.1.3 Design Principles and Bioinspiration

From an engineering standpoint, soft robots are typically constructed using elastomeric and polymeric materials whose mechanical properties are closer to those of biological tissues than to those of metals. Common structural materials include silicone rubbers and polyurethanes, which offer large elastic strains, resilience, and ease of fabrication through casting and molding processes [28]. Depending on the application, hydrogels and other soft polymer networks may also be employed, particularly when biocompatibility and gentle interaction are required. In addition to these passive matrices, soft robotic systems often integrate structural reinforcements—such as fibers, fabrics, or locally stiffer constraint layers—to tailor deformation patterns and enable directional motion under actuation [28, 29].

1.2 Octopus arm as a Paradigm for Dexterious Robotic Arms

1.2.1 Biological Principles

Among biological systems, the octopus arm represents a paradigmatic example of a soft structure that has been used to develop highly dexterious robotics counterparts. Unlike vertebrate limbs, octopus arms lack rigid skeletal elements and are instead classified as *muscular hydrostats* , a class of biological structures composed almost entirely of densely packed, incompressible muscle tissue [30, 31]. In muscular hydrostats, movement and force generation arise from coordinated muscle contractions operating under the constraint of an approximately constant volume, allowing complex deformations without the need for articulated joints. A schematic representation of a muscular hydrostat and its internal organization is shown in (Fig. 1.5).

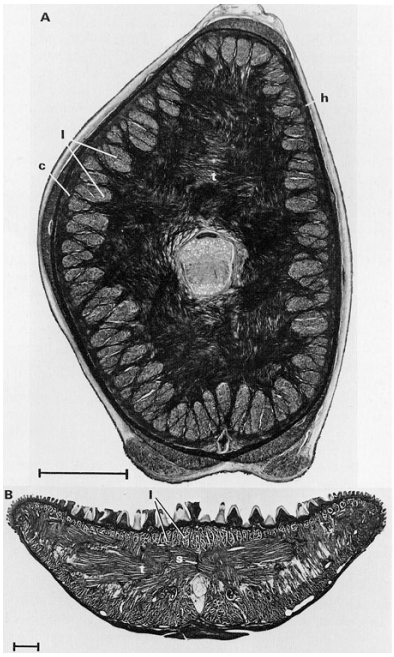

Figura 1.5: Examples of muscular hydrostats. (A) Transverse section of a squid tentacle stalk showing the arrangement of muscle fibres: transverse muscle fibres (t), longitudinal muscle fibres (l), circular muscle layer (c), and helically arranged muscle fibres (h) surrounding the axial nerve cord. (B) Transverse section of a cat tongue illustrating a similar muscular hydrostat organization. Adapted from [30].

This biological structure is found in several animal species, including squid tentacles, elephant trunks, and vertebrate tongues, each adapted to perform specific

functional tasks such as manipulation, grasping, or protrusion [30, 32].Among biological muscular hydrostats, the octopus arm stands out for its remarkable versatility. It can elongate, shorten, bend, twist, and locally stiffen while interacting safely with objects of different shapes, sizes, and compliance.

The arm is composed of a complex arrangement of muscle fibers embedded within connective tissue, forming a continuous and highly deformable structure along its entire length [33]. Unlike vertebrate limbs, it lacks rigid skeletal elements and belongs to the class of muscular hydrostats, biological systems in which movement and force generation arise from coordinated muscle contractions acting under the constraint of nearly constant internal volume.

These characteristics enable a wide repertoire of movements and a high degree of adaptability when interacting with the surrounding environment. For this reason, the octopus arm has become an important biological model for the design of soft robotic and continuum manipulators [9, 26].

1.2.2 Muscles

The internal musculature is organized into distinct muscle groups with different orientations, whose spatial arrangement can be clearly observed in transverse sections of the arm (Fig. 1.6). Three main muscle fiber orientations can be identified: longitudinal, transverse, and oblique.

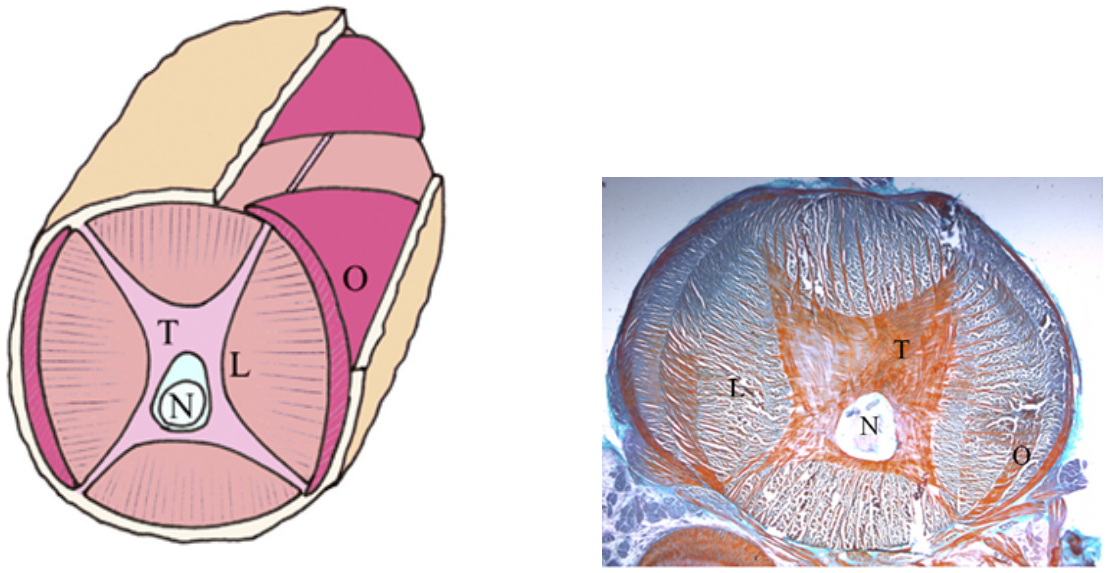

(a) Simplified schematic of the octopus arm muscular hydrostat.

(b) Histological cross-section of an octopus arm showing muscle bundles.

Figura 1.6: Organization of muscle groups in the octopus arm. Longitudinal (L), transverse (T), and oblique (O) muscles surround the central axial nerve cord (N).

Longitudinal muscle fibers run parallel to the main axis of the arm and are primarily responsible for arm shortening and bending. When these fibers are activated asymmetrically on one side of the arm, they generate localized shortening that produces curvature and bending of the structure.

Transverse muscle fibers encircle the arm radially. When they contract, they reduce the cross-sectional area of the arm. Due to the constant-volume constraint typical of muscular hydrostats, this radial contraction results in elongation of the arm.

Oblique muscle fibers are arranged helically around the arm and contribute to torsional movements as well as fine modulation of arm stiffness.

In addition to muscle fibers, connective tissue networks provide structural integrity, elastic energy storage, and resistance to excessive deformation. Ultrasound-based observations further support the mechanical relevance of connective tissue trabeculae and the intimate coupling between muscle arrangement and measured echo-intensity patterns, consistent with a functional role in stiffness modulation and load transmission [34]. Quantitative morphological analyses have further shown that several parameters, including arm diameter, sucker diameter, and internal volumes associated with muscular and neural elements, vary along the longitudinal axis of the arm (Fig. 1.7) [35]. These variations indicate that the arm is not mechanically uniform along its length and suggest that different regions may

contribute differently to manipulation tasks.

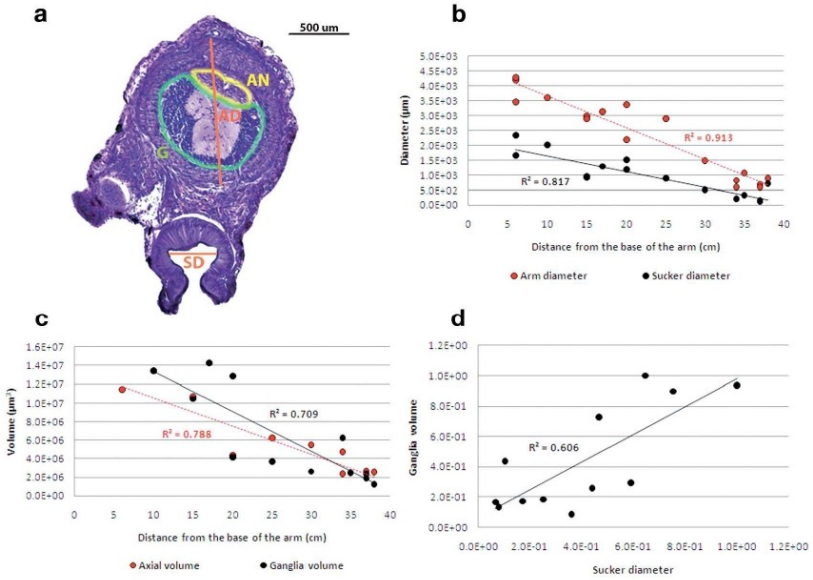

Figura 1.7: Morphological analysis of the octopus arm. (a) Transverse section with identification of anatomical regions; (b–d) variations of arm diameter, sucker diameter, axial muscle volume, and ganglia volume along the longitudinal axis of the arm (adapted from [35]).

Functionality: The combination of the three-dimensional muscle architecture and the constant-volume constraint allows the octopus arm to generate a wide range of continuous deformations, including bending, elongation, shortening, and torsion. The principal deformation mechanisms arise from the coordinated activation of the different muscle groups. Bending is mainly generated through unilateral activation of longitudinal muscles, producing local shortening on one side of the arm while the opposite side remains elongated. Elongation and shortening result from the coordinated interaction between longitudinal and transverse muscles, whereas torsional movements are enabled by the activation of oblique muscle fibers arranged helically around the arm. These deformation mechanisms, governed by the constant-volume constraint, are schematically illustrated in Fig. 1.8 [30, 31].

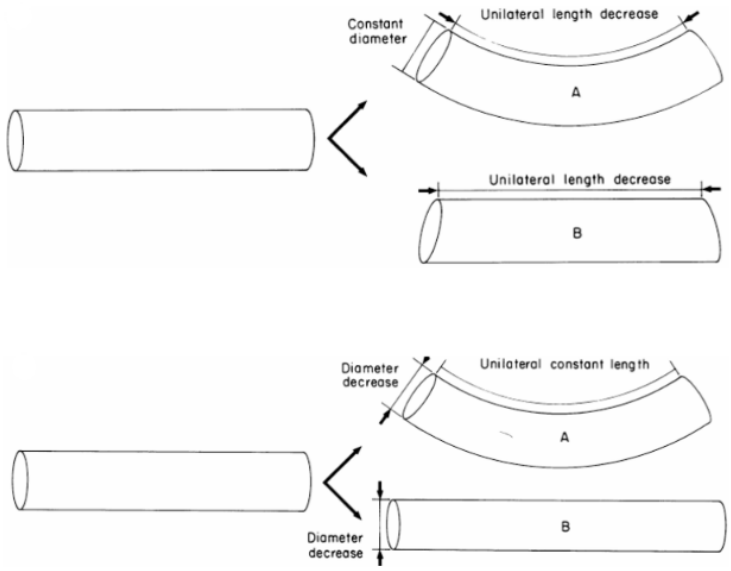

Figura 1.8: Mechanisms of bending and elongation in muscular hydrostats. Unilateral contraction of longitudinal muscles induces bending, while coordinated contraction of transverse muscles leads to elongation under constant-volume constraints (adapted from [30]).

Octopus arms are also capable of remarkable elongation. During reaching movements, they can extend to more than twice their reference length. Moreover, elongation performance depends on individual characteristics, such as body size and sex, as well as on the specific arm used for the task [36]. These observations suggest that biomechanical and morphological factors influence arm-use strategies and motor performance.

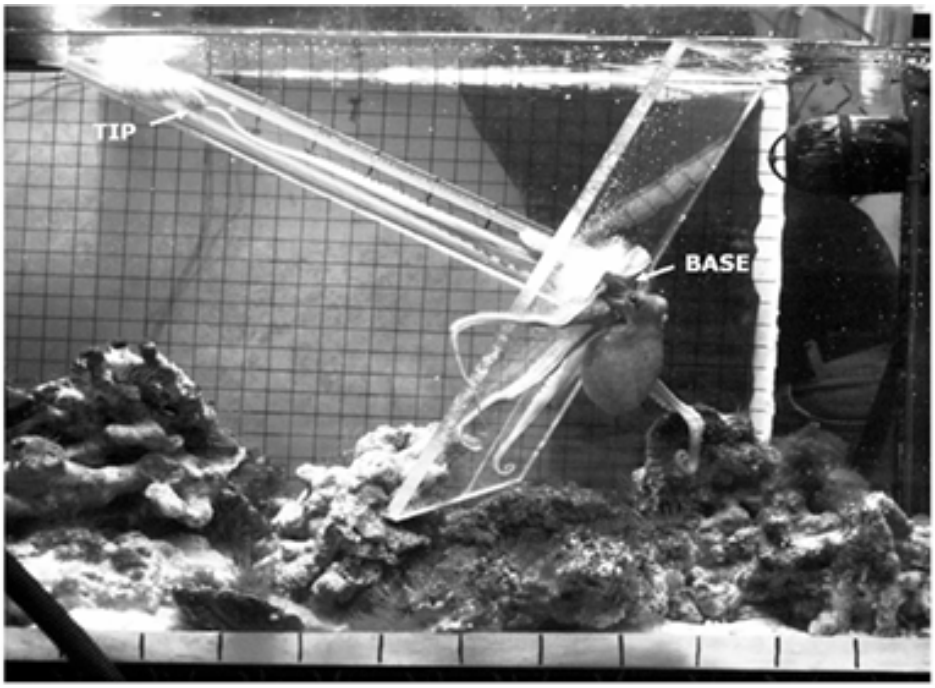

Figura 1.9: Experimental setup for in vivo measurement of arm elongation during reaching. A graduated tube constrains the arm to extend toward a bait target, enabling direct quantification of elongation capability (adapted from [36]).

1.3 Octopus-inspired Soft Robotic Arms

1.3.1 Principles exploit from nature

The distinctive morphological and functional characteristics of the octopus have made it a paradigmatic biological model for the development of soft robotic systems. In particular, the octopus arm represents a unique example of a biological manipulator capable of performing complex reaching, grasping, and manipulation tasks without the support of rigid skeletal elements. This remarkable dexterity is achieved through the muscular hydrostat architecture, in which densely packed muscle fibers arranged in longitudinal, transverse, and oblique orientations enable bending, elongation, shortening, torsion, and variable stiffness along the entire arm length [30, 32].

From an engineering perspective, the octopus arm embodies several properties that are highly desirable for robotic manipulation in unstructured and uncertain environments, such as continuous deformation, intrinsic compliance, adaptability to external constraints, and the ability to distribute contact forces over large surface areas. These features have motivated extensive interdisciplinary research aimed at

translating the biological principles underlying octopus arm function into artificial systems [37].

A key conceptual framework supporting this bio-inspired approach is the notion of embodied intelligence, according to which intelligent and adaptive behavior emerges not solely from centralized control strategies, but from the dynamic interaction between body morphology, material properties, control architecture, and the environment. In the octopus, the tight coupling between soft body mechanics and distributed neural control allows the animal to simplify motion generation and interaction with the environment, effectively offloading part of the control complexity to the physical structure of the body itself. This principle has strongly influenced the design philosophy of soft robotic systems inspired by the octopus arm [38].

1.3.2 Materials and Actuation Technologies

Soft robotic manipulators rely on a variety of actuation technologies to generate motion within compliant structures. Common approaches include pneumatic or hydraulic actuation, cable-driven mechanisms, shape memory alloy (SMA) actuators (Fig. 1.11), and electroactive polymers (EAPs) (Fig. 1.10). These strategies exploit different physical principles to produce deformation in soft materials while maintaining structural flexibility and enabling safe interaction with the surrounding environment [1, 39].

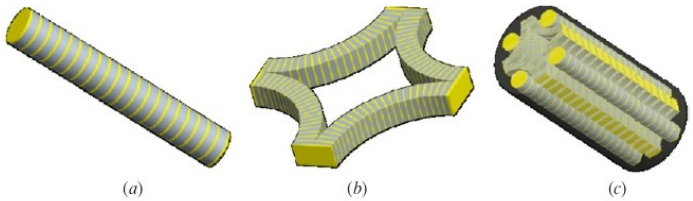

Figura 1.10: Conceptual design of a robotic muscular hydrostat inspired by the octopus arm. (a) Cylindrical longitudinal actuation elements running along the arm length. (b) Transverse actuation elements arranged orthogonally to the longitudinal ones. (c) Integrated structure combining longitudinal and transverse elements to reproduce deformation modes such as bending, elongation, and shortening. Adapted from [40].

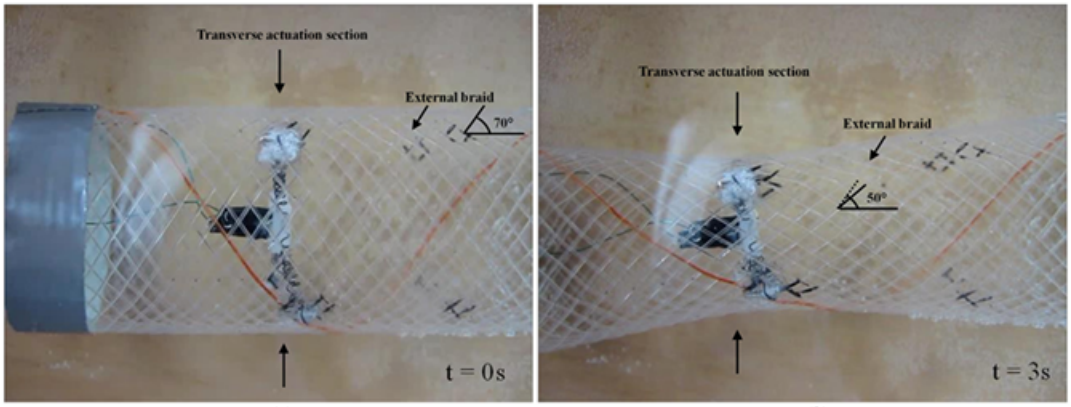

Figura 1.11: Behaviour of a cylindrical unit composed of a silicone structure reinforced by an external braided sleeve and actuated by transverse SMA coils. The radial contraction of the transverse actuator reduces the diameter of the structure and, due to the constant-volume constraint, produces axial elongation. (a) Initial configuration (t = 0 s) with braid fibre angle of approximately 70° relative to the longitudinal axis. (b) Activated configuration (t = 3 s) in which the actuator reduces the diameter of the structure, producing elongation and decreasing the braid fibre angle to approximately 50°. Experimental measurements show that a 20% reduction in diameter results in about 90% elongation (adapted from [41]).

Cable-driven actuation Among the different actuation strategies employed in soft robotics, cable-driven actuation has been widely adopted in octopus-inspired robotic arms due to its mechanical simplicity, reliability, and ability to generate distributed bending along compliant structures. In these systems, tendons are embedded within soft bodies and routed along the arm at a certain radial distance from the central axis, typically being anchored near the distal region in order to generate curvature through asymmetric cable tension [42, 43] (Fig. 1.12).

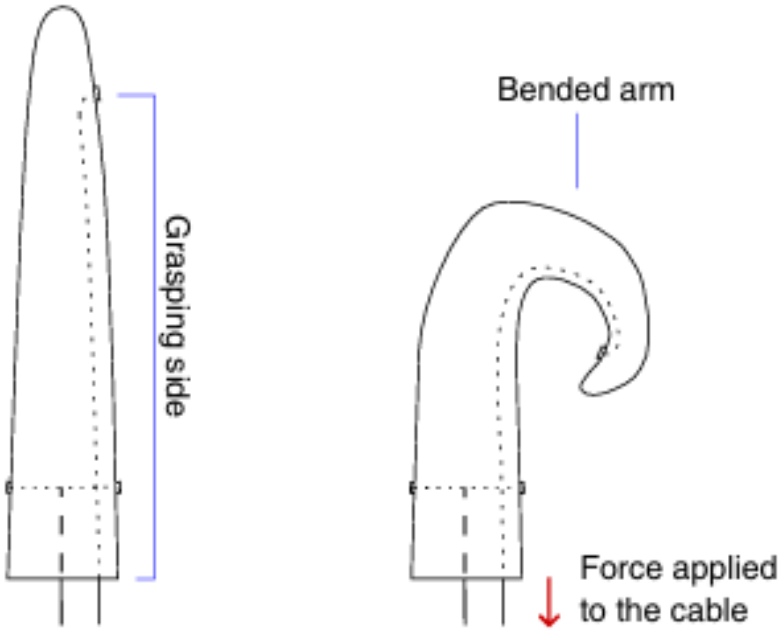

Figura 1.12: Time sequence illustrating the curling and extension of an octopus-inspired soft robotic arm in water. The images highlight the distributed curvature and continuous deformation along the arm during actuation (adapted from [43]).

Cable placement The position of the cable within the structure plays a fundamental role in determining the resulting deformation. In cable-driven continuum manipulators, tendons are typically routed at a certain radial distance from the neutral axis of the structure. When tension is applied to the cable, this offset generates a bending moment that induces curvature in the manipulator. By coordinating multiple tendons arranged around the body of the arm, it becomes possible to control both the direction and magnitude of bending. Similar actuation principle is widely employed in tendon-driven continuum robots, where cables routed along a flexible backbone generate distributed deformation of the structure [44, 45].

Cable type and mechanical properties To achieve large and controllable deformations while preserving structural integrity, many soft robotics projects use highly compliant elastomeric materials, such as silicone, within which low-elasticity cables are integrated, for example, nylon fishing lines. These elements allow efficient transmission of tensile forces and precise control of deformation.

In some cases, the system may also include elastic elements, such as rubber bands, or structural reinforcements such as braided sleeves or embedded fibers [41]. The introduction of such components modifies the mechanical response of the

structure, increasing the overall compliance of the system and allowing smoother deformations.

These design strategies allow the creation of soft manipulators capable of generating continuous curvatures and complex spatial configurations, while at the same time maintaining safe interaction with the surrounding environment.

Embedded routing In many soft robotic designs, cables are embedded directly within elastomeric structures during fabrication. Embedding allows forces to be distributed along the manipulator body while maintaining a compact design and protecting the cable from external interference. At the same time, the interaction between the cable and the surrounding material can introduce friction, which affects force transmission and may influence the repeatability of motion.

Passive behavior Cable-driven systems may also contribute to passive mechanical behaviors within the structure. Depending on the routing configuration and material properties, the manipulator may exhibit passive restoring forces that assist in returning the structure toward its original configuration. This passive contribution can be beneficial in soft robotic systems, as it reduces the need for continuous actuation and can improve energy efficiency while maintaining mechanical simplicity.

Hysteresis and design limitations Despite their advantages, cable-driven soft robotic systems present several limitations. Friction between the cable and the surrounding elastomeric material, combined with the viscoelastic properties of soft polymers, can lead to hysteresis effects in which loading and unloading phases follow different deformation paths. This phenomenon may reduce motion repeatability and control precision, particularly during cyclic actuation.

Additionally, the routing and integration of cables within soft structures may introduce fabrication challenges and potential wear over time. For these reasons, the design of cable-driven soft manipulators requires careful consideration of cable type, placement, and integration within the compliant structure in order to balance actuation performance, durability, and controllability.

1.3.3 Limitations in the current approaches

Despite their effectiveness, cable-driven soft manipulators have several limitations. One major challenge concerns the integration of tendons within highly deformable materials, where the friction between the cable and the surrounding structure can reduce actuation efficiency and lead to non-uniform curvature along the arm. Furthermore, tendon routing often ends before reaching the distal tip of the manipulator to avoid structural damage or excessive stress concentrations. As a

result, the distal region frequently remains largely passive (Fig. 1.13), limiting the system's ability to reproduce the fine manipulation capabilities observed in the biological arms of the octopus. A further limitation concerns the difficulty of achieving precise control of distributed deformation. Since cable-based actuation typically generates curvature by shortening only one side of the structure, the resulting movement may not fully replicate the coordinated muscle activations that occur in biological muscular hydrostats.

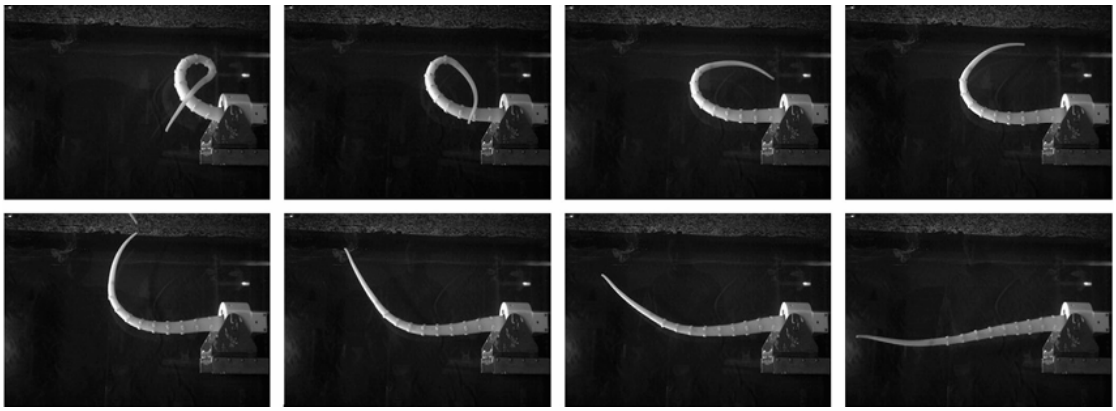

(a)

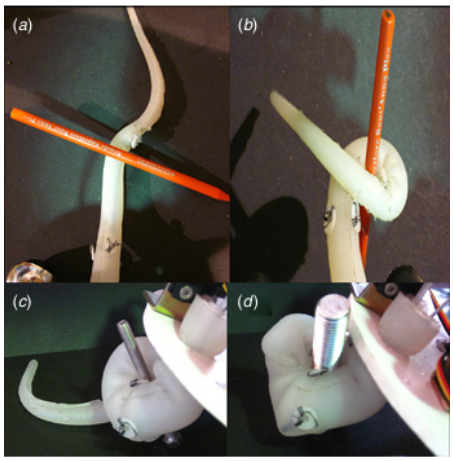

(b)

Figura 1.13: Examples of bending octopus-inspired soft robotic arms with passive distal tips. (a) Time sequence showing the bending and extension of a silicone soft arm during actuation (adapted from [41]). (b) Example of grasping with an object using a cable-driven soft arm where the distal tip remains passive (adapted from [43]).

1.4 Motivation for Thesis

Within this context, the present thesis pursues two main research objectives.

The first objective is to investigate alternative actuation strategies for soft robotic arms inspired by the octopus. In particular, different types of actuation elements were integrated within the body of the soft arm in order to evaluate how the internal structure influences the resulting motion, with specific attention to the curvature

The second objective is to study the biological behavior of the octopus arm in order to better understand the mechanical and functional role of the distal tip. While the distal region is often left passive in many octopus-inspired robotic arms, its role in biological grasping behavior remains not fully understood. Through experimental observations of octopus arm interactions, this work investigates whether the tip behaves as a purely passive element, whether it exhibits distinct motion patterns, or whether it contributes actively to the grasping process. Insights derived from these biological observations are then used to inform the design of a soft robotic arm in which the distal region is explicitly considered in the mechanical design, with the aim of improving the reproduction of biologically inspired grasping strategies.

Capitolo 2

Biological Experiments on Octopus Arm Behavior

2.1 Introduction

Biological systems provide a fundamental source of inspiration for the development of soft robotic manipulators. In particular, studying how animals exploit compliance, distributed actuation, and morphology to achieve dexterous manipulation allows the identification of functional behaviors that can be adapted to the robotic structure under development. Beyond material selection and prototype fabrication, systematic observation of the biological model plays a crucial role in guiding design choices.

In this context, and in collaboration with the Acquario di Genova, a series of behavioral experiments on octopuses was conducted to investigate arm use during object interaction and grasping. The experimental analysis focused on the distal region of the arm, not as an isolated grasping unit, but as a key observable segment to study the coordination between the arm tip and the rest of the arm during grasp formation. In particular, the distal region was analyzed to assess whether its motion exhibits a predominantly passive behavior—moving as a consequence of the global arm deformation—or whether it displays independent or locally driven dynamics.

This chapter describes the experimental environment, acquisition setup, and protocol adopted during the trials. It then presents the main experimental results, focusing on recurring behavioral and kinematic patterns observed during distal arm interaction. Finally, the biological findings are summarized and interpreted in terms of design-relevant implications, providing a bridge toward the development of octopus-inspired soft robotic arms.

2.2 Methods

2.2.1 Experimental Environment and setup

Animal conditions

Experiments were conducted on three octopus species, each housed in a dedicated tank appropriate to its size and behavioral needs:

- *Octopus vulgaris*: tank dimensions 260 × 80 × 100 cm
- *Enteroctopus dofleini*: tank dimensions 420 × 220 × 280 cm
- *Octopus maya*: tank dimensions 120 × 80 × 60 cm

The experiments were conducted following the daily husbandry schedule of the aquarium. A typical experimental morning involved sequential observations of the three species in the order *Enteroctopus dofleini* / *Octopus vulgaris* – *Octopus maya* – *Octopus vulgaris* / *Enteroctopus dofleini*. *Enteroctopus dofleini* and *Octopus vulgaris* were fed three times per week, whereas *Octopus maya* was fed daily.

All trials were carried out during regular husbandry activities and followed the standard animal care protocols of the hosting aquarium. Observations were typically performed early in the morning (around 08:00), coinciding with feeding time, when the animals were generally more responsive and interactive. This facilitated the observation of reaching and grasping behaviors during object interaction.

Data acquisition setup

To capture the movement of the arm and the interaction with objects, a two-camera acquisition system was used. A Nikon camera was positioned in front of the octopus to observe in detail the bending and curvature dynamics of the arm, allowing an accurate view of the distal region of the arm during interaction with objects.

In parallel, a fixed Logitech webcam was positioned laterally to the aquarium to capture a wider view of the experimental scene and provide contextual information about the overall interaction between the animal and the objects.

Due to differences in tank geometry and experimental layout, the position of the cameras varied slightly depending on the species and tank configuration, as illustrated in Fig. 2.1. In particular, the Nikon camera was positioned at approximately 76 cm height and 76 cm distance from the tank for *Enteroctopus dofleini*, 92 cm distance and 124 cm height for *Octopus vulgaris*, and 135 cm height and 240 cm distance for *Octopus maya*.

(a) *Octopus vulgaris*

(b) *Octopus maya*

(c) *Enteroctopus dofleini*

Figura 2.1: Aquarium environments used for the experiments with the three species: (a) *Octopus vulgaris*, (b) *Octopus maya*, and (c) *Enteroctopus dofleini*. The photographs illustrate the tanks and surrounding experimental areas where behavioral recordings were performed.

Interaction elements

To elicit reaching, curling, and grasping behaviors, both food stimuli and manipulable objects were employed. The food stimuli consisted of fish or crustaceans, while the objects used for interaction included rope (Fig. 2.2b), plastic jar (Fig. 2.2a) , feeding tubes commonly used by aquarium biologists, and two spherical objects (balls) with different surface textures (one smooth and one rough) (Fig. 2.2c),used to examine how surface properties influenced arm-tip adhesion.

(a) **(b)** **(c)**

Figura 2.2: Interaction elements used during the experiments: (a) rigid plastic jar (7.1 cm diameter × 8.5 cm height), (b) braided polypropylene rope (10 mm diameter, 10 m length), (c) sponge balls (7 cm diameter each).

The objects were presented using different methods depending on their physical properties and the experimental purpose. Whenever possible, they were suspended at a controlled height within the aquarium to encourage arm extension into free space. Feeding tubes were frequently used, as octopuses tend to spontaneously attach to and manipulate them, providing repeatable and biologically relevant interaction scenarios.

Lightweight spherical objects could not be suspended due to their buoyancy and were therefore manually introduced into the water by the aquarium biologists. In some trials, these objects were gently set in motion through manual movements in the water to stimulate exploratory responses. Two types of spheres were used: one with a smooth surface and one with a rough surface.

2.2.2 Experimental protocol

Each experimental session consisted of a sequence of trials conducted according to the following procedure:

1) *Activation*: the octopus was initially stimulated using food delivered through a feeding tube to promote active engagement. (Fig. 2.3)

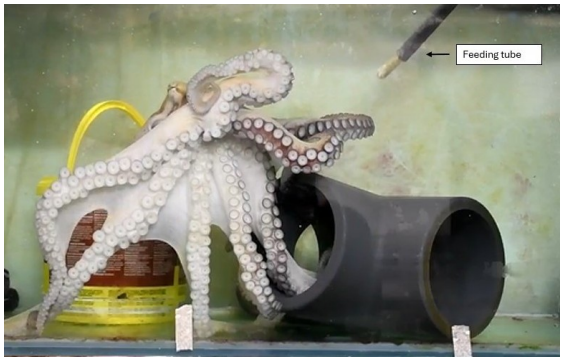

Figura 2.3: Activation phase of the experimental protocol: The octopus is fed by a tube with a shrimp attached at the tip.

2) *Object presentation*: once the animal was active and alert, the selected object was introduced into the tank according to the planned modality (suspended or manually released, depending on its physical properties). The octopus was then allowed to freely approach, explore, and interact with the object. (Fig. 2.4)

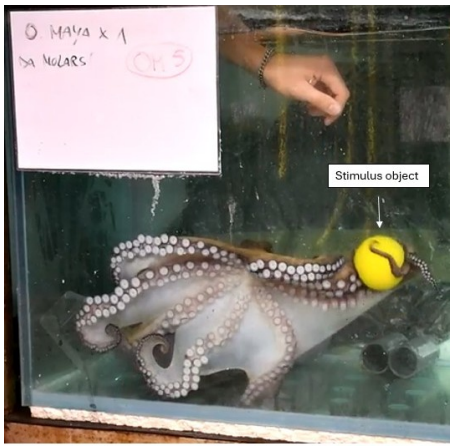

Figura 2.4: Object presentation phase: manual introduction and dynamic manipulation of a spherical object to stimulate grasping behavior in response to a moving target.

3) *Low-interest condition*: if the object was ignored, food was occasionally placed inside or attached to it to increase attractiveness. A known limitation of this approach is that the octopus may pull the object under the mantle, reducing visibility and preventing reliable observation of distal arm motion.(Fig. 2.5)

Figura 2.5: Low-interest condition: a shrimp is placed inside the object to increase its attractiveness when the octopus initially ignores the stimulus.

4) *Recording*: both cameras recorded each trial. Manual annotations included latency to first contact, contact duration, grasp modality, and trial outcome. (grasp success or failure).

2.3 Results

The experimental results are presented in terms of aggregated behavioral observations derived from video analysis of analyzable trials. Rather than reporting trial-by-trial measurements, the focus is placed on identifying recurring interaction patterns and context-dependent strategies adopted by the octopus arm during object exploration and grasping. Particular attention is given to how different regions of the arm are recruited depending on object properties and interaction dynamics.

Video analysis revealed that the initiation of grasping behavior is not governed by a fixed sequence, but instead depends on object geometry, accessibility, and spatial context. When interacting with small (Fig. 2.10), distant, or partially enclosed objects, such as items located inside boxes or narrow containers, exploration and grasping were frequently initiated by the distal tip. In these cases, the distal region exhibited localized bending and fine exploratory movements, enabling access to confined spaces.

Conversely, when interacting with large, elongated, or easily accessible objects, initial contact often occurred through sucker attachment of the mid-arm region, while the remaining portion of the arm remained curled. As interaction progressed, the arm gradually uncurled and extended along the object, with suckers attaching sequentially as the animal explored or pulled the object toward the body.So grasp configuration depend on object size, geometry, and the functional context of interaction

When interacting with moving objects, the octopus frequently adopted faster and more abrupt arm movements compared to those observed during interaction with stationary objects. In these dynamic conditions, the arm often performed rapid and highly regular curling motions, resulting in near-perfect circular or spiral configurations. These movements appeared optimized for intercepting and enclosing a moving target rather than for detailed shape adaptation. In addition, moving objects were often approached using multiple arms simultaneously, suggesting a coordinated capture strategy aimed at increasing enclosure efficiency.

Surface properties also strongly influenced the interaction strategy. Smooth spherical objects were frequently grasped through effective sucker attachment, whereas rough-surfaced spheres did not allow effective suckers adhesion. As a consequence, the octopus shifted its strategy and relied predominantly on arm wrapping and whole-arm enclosure to grasp the object. Infact, as we can see in Fig. 2.10 the ball is not attached to the suction cups, but he grabs it because the roughness of the ball does not allow it to stick.

In contrast, when exploring stationary objects, the arm exhibited slower, continuous, and highly adaptive movements. The distal region tended to closely follow the shape of the object, resulting in arm configurations that varied significantly depending on object geometry. Stationary objects were more frequently explored using a single arm, indicating a more localized and fine-tuned interaction strategy focused on detailed exploration rather than rapid capture.

Despite the variability in exploration strategies, a consistent functional organization along the arm emerged across trials and species. The mid and proximal portions of the arm primarily contributed to object stabilization through sucker attachment, while the distal region was selectively recruited for fine exploration and shape adaptation when required.

In several trials involving both *Enteroctopus dofleini* and *Octopus maya*, the proximal or mid-arm region stabilized the object, while the distal tip explored the object interior (Fig. 2.6) or surface details. Notably, the distal tip appeared extremely soft and compliant, capable of closely following object contours. However, when external forces were applied, the same region exhibited high resistance, indicating a non-linear mechanical behavior that combines conformability with robustness.

Figura 2.6: The octopus inserts the distal arm tip into the test tube to actively explore its interior.

Regardless of object interaction, the distal tip frequently exhibited continuous and fluid motion even in the absence of contact. This observation indicates that distal arm elasticity is an intrinsic property rather than a passive to object constraints.

In multiple trials, the distal region was observed to remain curled on the side opposite (Fig. 2.7) to the interaction surface during active exploration that did not directly involve the distal tip. This persistent curvature may reflect a passively stable or mechanically preferred resting configuration requiring minimal active neuromuscular effort. Alternatively, it could represent a protective or defensive posture, with the suckers oriented outward and ready for rapid engagement.

Figura 2.7: Example of persistent distal curvature with exposed suckers during non-contact arm motion.

A representative example of this behaviour during interaction with the food delivery tube is shown in Fig. 2.8. The arm initially engaged the tube through proximal suction cup attachment while the distal portion remained curled on the opposite side. As the interaction progressed, the distal region gradually uncoiled, contributing to a more complete wrapping of the object.

Figura 2.8: Time sequence of arm interaction with the food delivery tube in *Enteroctopus dofleini*. At $t = 0$ s the arm attaches to the tube using proximal suckers while the distal region remains curled on the oppiste side. During continued interaction ($t = 1$–6 s) the distal portion progressively uncurls and extends, contributing to a more complete wrapping of the object. Arrows indicate the distal arm tip.

A similar exploratory behavior of the distal arm region was also observed in *Octopus maya*, as shown in Fig. 2.9. In this case, the arm not only uncurls along the object but also moves around it, exploring the tube from the opposite side.

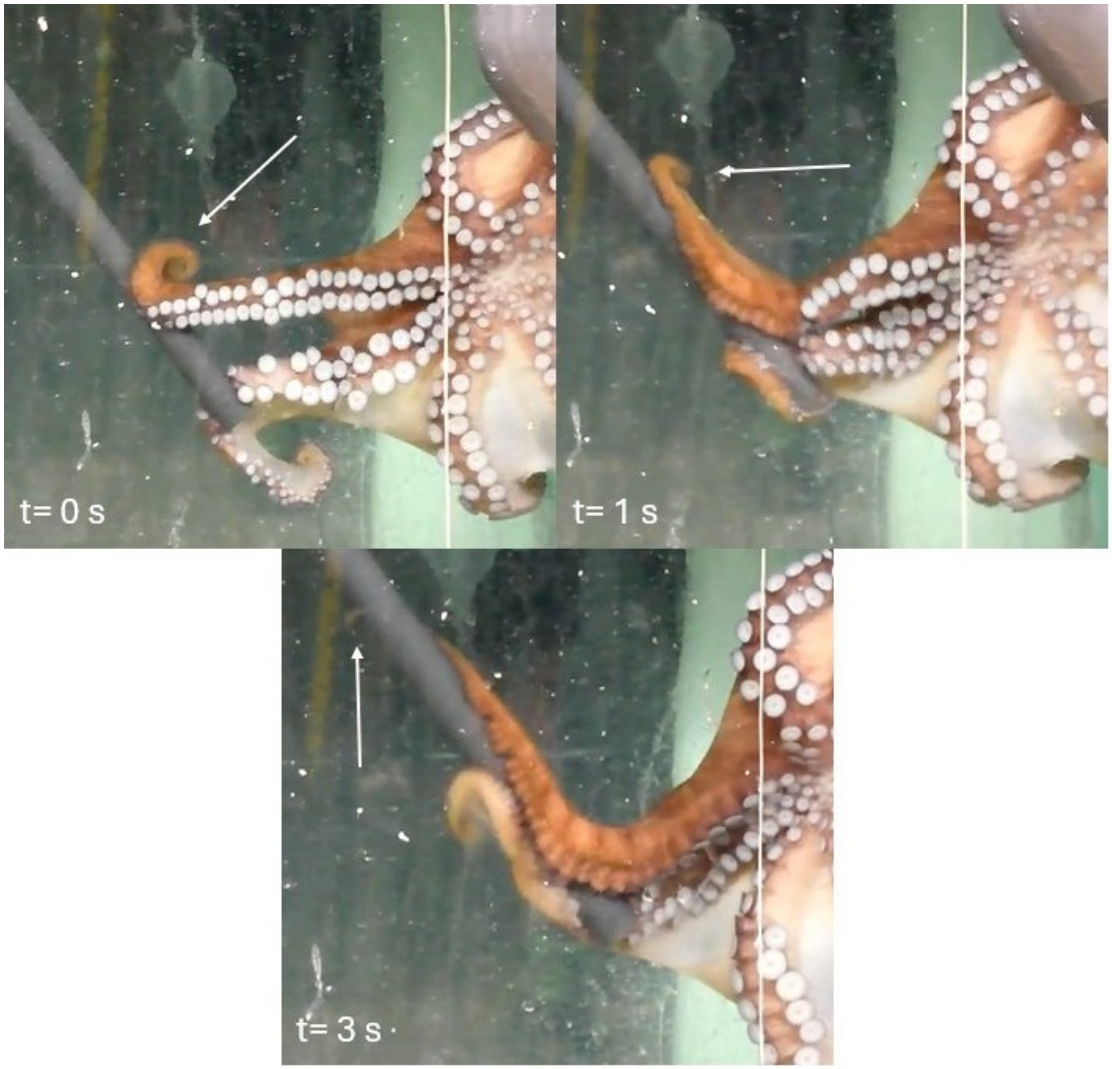

Figura 2.9: Time sequence of arm interaction with the food delivery tube in *Maya*. At $t = 0$ s the distal portion of the arm is curled while approaching the tube. At $t = 1$ s the arm extends and begins to uncoil along the object. At $t = 3$ s the distal tip moves around the tube, exploring the object from the opposite side. Arrows indicate the distal arm tip.

During arm retraction, particularly evident in trials involving *Enteroctopus doflein*, the arm often shortened through an accordion-like mechanism. Rather than retracting through simple bending, the arm locally compressed and thickened along its length, enabling axial shortening while maintaining contact with the object. This behavior is likely enabled by the dense three-dimensional muscular architecture of the arm, characteristic of a muscular hydrostat, in which coordinated activation of

longitudinal and transverse muscle groups allows axial shortening while preserving volume.(Fig. 2.10)

Figura 2.10: Time sequence illustrating arm retraction during interaction with the object in *Enteroctopus Dofleini*. (a) Extended configuration prior to retraction ($t = 0$ s). (b) Retraction phase ($t = 1$ s), showing axial shortening and local thickening of the arm while maintaining contact with the object, consistent with a muscular hydrostat mechanism.

2.4 Functional Interpretation and Design-Relevant Implications

The experimental observations indicate that octopus arm behavior relies on a repertoire of interaction modes rather than a single grasping strategy. The arm exhibits different movement patterns depending on object geometry, surface properties, motion, and interaction context.

To provide a concise synthesis of the main findings, the observed biological behaviors are summarized and interpreted in terms of their functional relevance for artificial systems. Table 2.1 reports the key experimental observations and outlines how each behavior can be translated into design principles for octopus-inspired soft robotic manipulators.

Experimental Observation	**Design Implementation in the Proposed Robotic Arm**
The distal tip exhibits high conformability and closely follows object contours during exploration.	Use of highly compliant materials in the distal region to preserve shape adaptability and soft contact behavior.
Proximal segments stabilize the object while the distal region performs fine adjustments.	Differentiated structural organization along the arm, combining tendon-driven bending for global motion with localized distal flexibility.
Arm retraction occurs through distributed axial shortening rather than pure bending.	Integration of braided sleeve reinforcements to guide deformation and support controlled axial compression during tendon actuation.
The entire arm (including the distal region) combines high conformability with resistance to external load.	A compliant segmented internal skeleton is introduced within the silicone body, designed to guide bending and improve structural robustness while maintaining overall softness.

Tabella 2.1: Summary of biological observations and their direct translation into structural and material design choices for the octopus-inspired soft robotic arm.

The synthesis reported in Table 2.1 highlights the apparent functional differentiation along the arm and the context-dependent role of the distal region. However, it is important to emphasize that the octopus arm operates as a continuous muscular hydrostat rather than as a structure divided into discrete functional units. The distal tip does not represent a separately controlled "hand-like" segment; instead, the entire arm is subject to distributed neuromuscular control.

The great fluidity observed at the distal end is therefore primarily related to its reduced diameter and mass, which mechanically allow higher curvature and finer motion, rather than to a fundamentally different control strategy. Across tasks, the arm exhibits coherent and integrated actuation, with variations in movement patterns emerging from geometry and interaction context rather than from strict functional compartmentalization.

These findings directly motivate the design choices discussed in the following chapters. Rather than directly replicating the biological structure of the octopus arm, these observations were used to identify movement patterns that could be beneficial to reproduce in a soft robotic manipulator. In many octopus-inspired soft robotic arms, actuation typically terminates before the distal tip, leaving the

final segment as a purely passive silicone extension. To date, limited attention has been devoted to systematically investigating the functional implications of this passive configuration.

The objective of this thesis is therefore to investigate the role of the distal tip during arm bending and object interaction, in order to better understand whether its behavior is primarily passive or actively controlled. The experimental observations presented in this work aim to clarify how the distal tip behaves in relation to the rest of the arm during grasping and bending. These insights are then used to inform the design of soft robotic arms that seek to reproduce key movement patterns observed in the animal—particularly the coordinated curvature that emerges during whole-arm bending—while preserving softness, flexibility, and mechanical robustness.

Capitolo 3

Design

3.1 Introduction

Following a targeted review of the soft robotics literature, which frames the motivations of the field and its main research directions, the design of an octopus-inspired soft robotic arm was initiated with the objective of developing a functional prototype [43, 46].

Octopus arms represent a paradigmatic example of soft biological manipulators, characterized by continuous deformation, high compliance, and the ability to generate complex grasping behaviours without rigid skeletal support [43, 46]. These properties have strongly motivated research on continuum and soft robotic arms for manipulation tasks in unstructured environments [9]. In addition to the global arm behaviour, the distal tip is treated as a dedicated design target. In biological octopus arms, distal segments are frequently involved in exploratory interactions, initial contact, and grasp initiation [43, 46]. Accordingly, the following design iterations focus on tailoring the mechanical response of the distal region to better support tip-driven manipulation.

3.2 Methods

A common baseline solution for octopus-inspired soft arms consists of a silicone continuum body embedding internal tendons routed along the arm length (Fig. 3.1). In this work, the tendons were implemented using nylon fishing lines and actuated by an external unit to generate bending.

The fishing lines are routed inside internal silicone tubes embedded within the silicone structure. These tubes prevent direct contact between the fishing lines and the surrounding silicone, reducing friction and allowing smooth sliding during actuation. Without such guiding elements, the tendon would interact directly with

the silicone body, increasing friction and reducing the controllability of the resulting deformation.

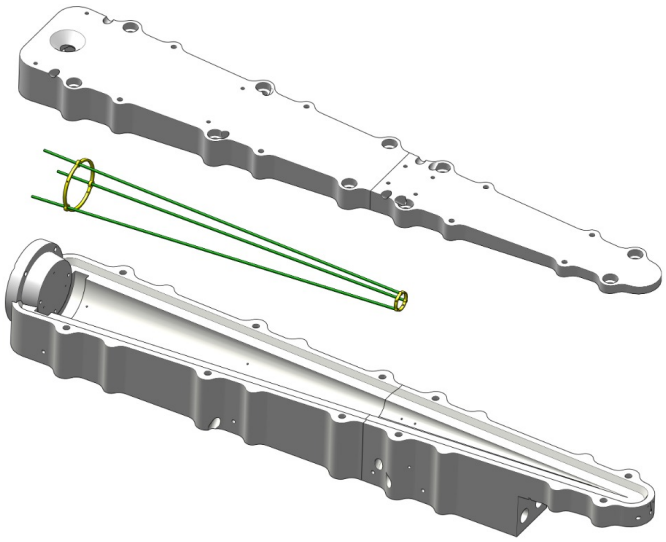

Figura 3.1: Braided sleeve (fiber 187-4600) used as internal reinforcement.

A three-tendon routing was adopted, with tendons arranged symmetrically around the cross-section and placed near the outer perimeter to increase the effective lever arm and improve achievable curvature. Dedicated supports were used to ensure repeatable tendon placement and alignment, and to position any internal inserts prior to casting. Once the internal components were correctly positioned, the mould was closed and filled with silicone Ecoflex 00-30 (Fig. 3.2) . The silicone was then left to cure for 4 hours before demoulding the final soft arm structure.

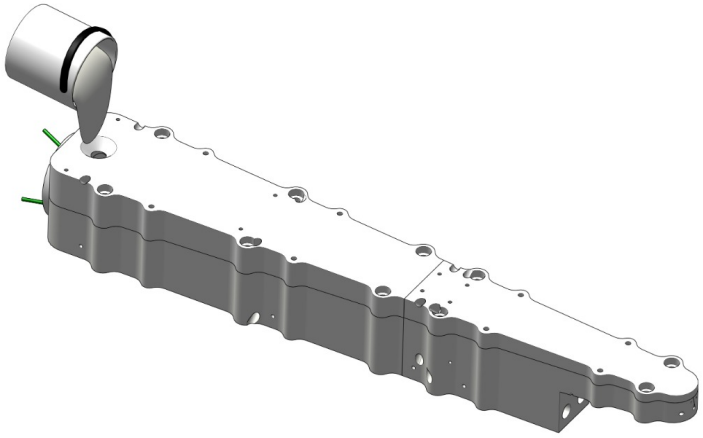

Figura 3.2: Braided sleeve (fiber 187-4600) used as internal reinforcement.

Building upon this baseline architecture, the present work investigates alternative internal elements and structural configurations aimed at improving bending behaviour, interaction capability, and force transmission. Particular attention is devoted to solutions that combine active tendon-driven actuation with favourable mechanical responses. In this study, fishing lines were inserted into guide tubes embedded in the silicone arm. Instead of using standard silicone tubes, different materials were tested for the guide elements in order to evaluate how their properties affect the bending and curvature behavior of the arm. Although the supports allow the symmetrical placement of three tendons around the cross-section of the arm, not all experimental configurations employed the full set of three tendons. Since the aim of this work was to study how different internal materials influence the mechanical behavior of the arm, some experiments were conducted using only one, two or three tendons.

This mold architecture allowed the testing of different internal configurations while maintaining the same external geometry of the arm. In particular, several experimental configurations were implemented by varying the internal elements and tendon arrangements in order to evaluate how different materials influence the bending behaviour and curvature of the arm.

3.3 Goal

The goal of this chapter is to investigate alternative design solutions for an octopus-inspired soft robotic arm, starting from a consolidated tendon-driven silicone

architecture. The study is organized around two main objectives, both aimed at improving curvature generation and grasping performance.

First, the work explores different materials and internal elements to be embedded within the silicone body in order to tune the arm mechanical response. In particular, the aim is to evaluate how these internal solutions affect bending efficiency, achievable curvature, force transmission, and grasp stability during object interaction.

3Second, the work focuses on the design and analysis of an active distal tip. Inspired by biological observations derived from video recordings and annotations of octopus arm grasping actions, this study investigates design principles that enable the distal region to support stable contact and effective wrapping. In particular, the objective is to promote the formation of a near-planar circular arc during grasping, improving adaptability and contact stability without significantly increasing control complexity.

Overall, the outcomes of this chapter provide the basis for a soft robotic arm in which active tendon actuation and tailored structural responses are effectively combined, with particular emphasis on enhancing distal grasping functionality.

3.4 Actuation mechanisms

3.4.1 Braided with silicone coating

The aim of these preliminary experiments was to evaluate how an internal structural element can influence the mechanical behavior of a soft robotic arm, particularly in terms of stiffness, elongation, and potential bending capability. The first concept was inspired by braided sleeves commonly used for cable insulation and by braided-sheath architectures widely adopted in soft actuators such as McKibben-type pneumatic artificial muscles, where the braid constrains and guides deformation [47]. The smallest braided sleeve available was selected (fiber 187-4600, diameter $\approx 3\,\mathrm{mm}$) .

Figura 3.3: Braided sleeve (fiber 187-4600) used as internal reinforcement.

An initial fabrication attempt used a 3D-printed PLA cylindrical mould to maintain alignment during casting and prevent the silicone from slipping off the sleeve. Although casting was successful, demoulding frequently damaged the external silicone layer, locally exposing portions of the braid. Fig. 3.4

(a) **(b)** **(c)**

Figura 3.4: Preliminary fabrication attempt using 3D-printed PLA tooling: (a) inner cylindrical core for sleeve alignment, (b) braided sleeve mounted on the core, (c) assembly placed inside an external cylindrical shell to contain the silicone during curing.

For this reason, I switched to a manual coating protocol. With the sleeve supported by a steel tube (Fig. 3.5),

Figura 3.5: Prototype of the first model: braided sleeve (fiber 187-4600) pre-coated with silicone and supported by a thin metal tube during fabrication.

silicone was applied using a thin brush in multiple layers while rotating the tube by hand to correct local sagging. Compared to pouring, this method provided better control of the deposited thickness, reduced air entrapment, and improved adhesion to the braid. Although the surface finish was not perfectly uniform, it reliably ensured continuous coverage, which was the main objective at this stage. The target coating thickness was approximately 2,mm along the entire length. The silicone was mixed at a 1A:1B ratio (50/50) and cured for approximately 4 hours at room temperature.

Following this protocol, three prototypes were produced using different silicone rubbers: Ecoflex 10, Ecoflex 20, and Ecoflex 30 (Fig. 3.3). Samples were cut into

5 cm segments and tested to evaluate force and elongation. Ecoflex 50 was also tested; however, due to its very low viscosity, it was difficult to handle and tended to form voids and air gaps during curing.

Tensile Test

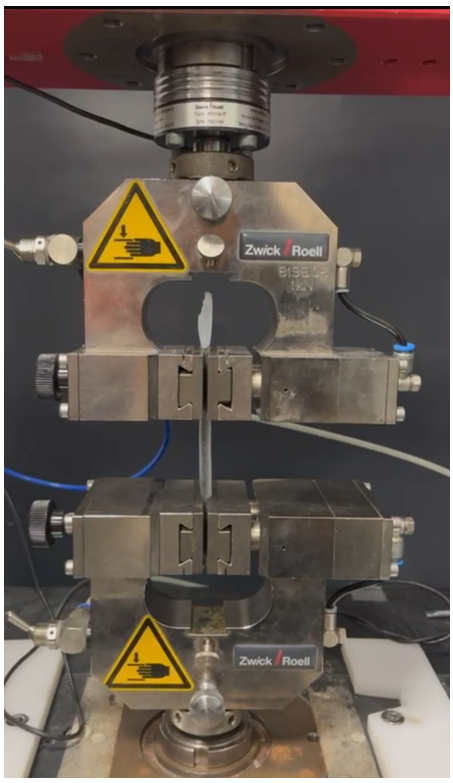

Figura 3.6: Initial tensile test setup

Tensile tests were performed using a Zwick/Roell universal testing machine equipped with a 1 kN load cell. Specimens were clamped between two metal grips and aligned to minimize eccentric loading and slippage. A monotonic tensile load was applied until failure, and force was recorded as a function of elongation.

For consistency across samples, the results are reported as force–extension curves (force as a function of elongation). Figure 3.7 shows representative responses for the tested materials.

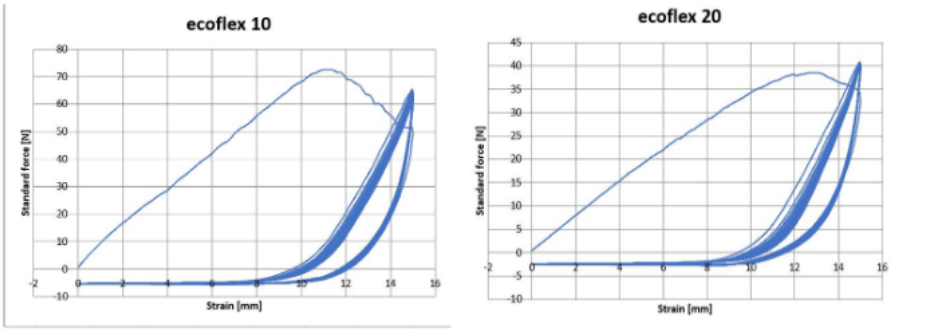

Figura 3.7: Ecoflex 10 and 20 graphs (force [N] vs strain [mm])

Ecoflex 10 exhibited a steeper initial response and a higher peak force (approximately 70–75 N), indicating a higher apparent stiffness. Ecoflex 20 reached a lower peak force (approximately 35–40 N) and sustained larger elongation before rupture, consistent with a softer and more compliant behavior.

A hysteresis loop is visible in both curves, reflecting viscoelastic energy dissipation typical of silicone elastomers. The loop appears more pronounced for Ecoflex 10, suggesting greater internal losses during loading–unloading, whereas Ecoflex 20 shows a smoother response and a more progressive recovery.

Ecoflex 00-10 was selected for the internal element because it is softer and more compliant than Ecoflex 00-20. As a result, the internal sleeve can bend more readily and does not excessively resist the tendon-driven deformation when the fishing line is pulled, helping the arm achieve larger curvature with lower actuation effort.

From a fabrication perspective, Ecoflex 00-10 also has a higher mixed viscosity, which was advantageous during coating: it reduced uncontrolled dripping and helped maintain a more consistent layer around the braided sleeve during curing.

Compression test in Ecoflex 10

Compression tests were performed using the same Zwick/Roell universal testing machine used for the tensile tests (1 kN load cell). The goal was to qualitatively evaluate the behavior of the Ecoflex 10 specimen under axial compressive loading.

Ecoflex 10 is highly compliant; therefore, in the first attempt the specimen buckled as soon as compressive force was applied, preventing a repeatable measurement (Fig. 3.8a). When the specimen was compressed manually over a smaller effective length, buckling was reduced and compression could be achieved more reliably. Based on this observation, the test was repeated using a reduced contact length (approximately 2 cm instead of the original 5 cm), leading to a stable compression of about 0.5 cm (Fig. 3.8b).

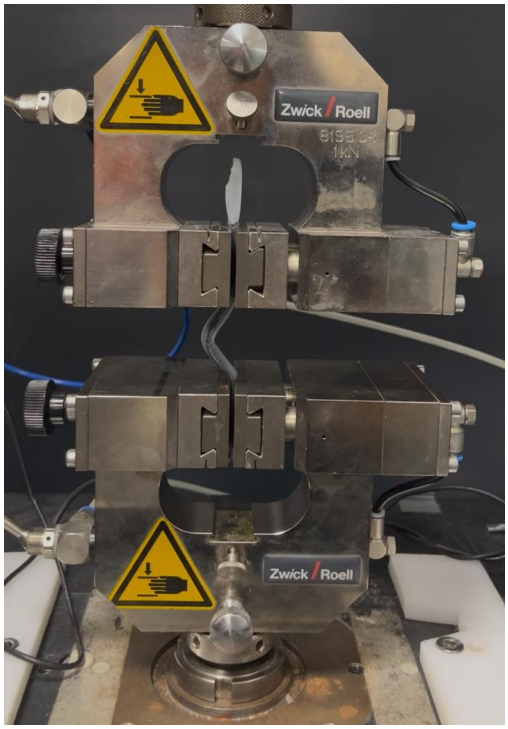

(a) Initial compression test setup: the Ecoflex 10 specimen buckled under axial loading.

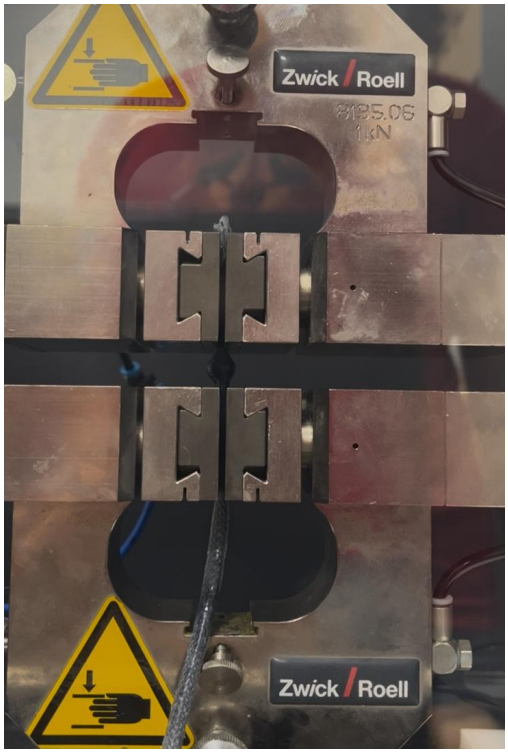

(b) Compression test with reduced contact length (about 2 cm), enabling stable compression.

Figura 3.8: Comparison of compression test configurations.

Figure 3.9 shows the force–displacement curve for specimen 2. An initial nonlinear region is observed, mainly due to settling of the specimen and contact stabilization at the grips. The curve then reaches a maximum load of approximately 10–14 N followed by a plateau, where the force remains nearly constant despite increasing deformation, which is consistent with the viscoelastic response of silicone elastomers. Beyond approximately 12 mm of displacement, the force increases again, which can be attributed to densification: as the structure becomes compacted, resistance to further compression rises. The three overlapping curves indicate good repeatability, with minor deviations likely caused by small differences in initial alignment and surface contact conditions.

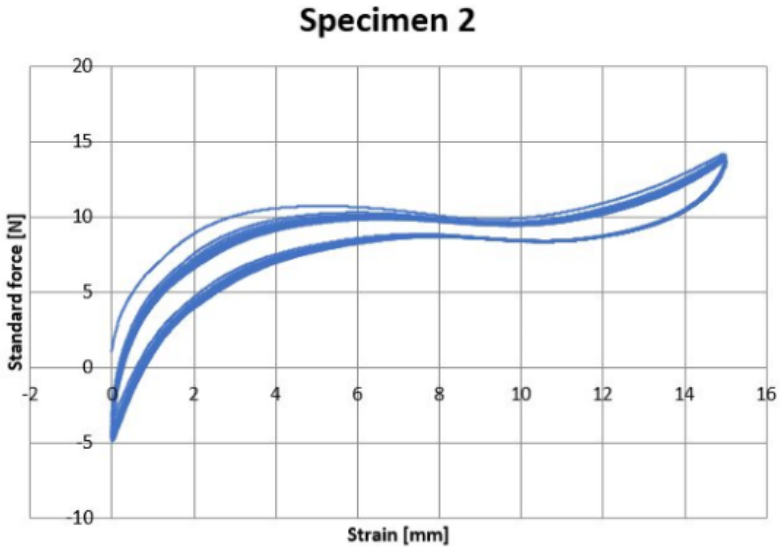

Figura 3.9: Compression test for specimen 2: force–displacement response (three repeated runs).

3.4.2 Design implications for the octopus-inspired arm

Overall, the tensile and compression tests support the feasibility of the silicone-coated braided sleeve as an internal reinforcement for the octopus-inspired soft arm. Ecoflex 10 was identified as the most suitable coating material, as it provides the required compliance for tendon-driven bending while offering improved processability during coating due to its higher mixed viscosity.

Compression tests highlighted that the primary constraint is not material failure but geometric instability (buckling) under axial loading when the effective unsupported length is large. This finding motivates the need for geometric guidance and/or encapsulation within the silicone body to stabilize the internal element and ensure repeatable behavior under combined loading during grasping.

3.4.3 Pneumatic

The fiber employed in the first design iteration of the octopus-inspired arm was further investigated as a candidate reinforcement for a McKibben-like Pneumatic Artificial Muscle (PAM). PAMs are contractile and/or extensible actuators driven by pressurized air: the inflation of an internal bladder generates an axial deformation that is mechanically constrained by an external reinforcement. By analogy with

biological muscles, PAMs are often arranged in agonist–antagonist pairs to obtain controlled motion.

To promote an extensible McKibben-inspired behavior, the original braided coil was mechanically re-shaped into a bellow-like profile. The procedure was inspired by the approach reported by Ansari et al. [48], where a braided sheath is deformed and subsequently heat-treated to stabilize (i.e., "memorize") the imposed geometry.

In the present work, the geometry modification was carried out as follows:

- a tube was used as a support to keep the braided structure aligned during forming;
- the coil was manually shaped to obtain a bellow-like profile along the longitudinal axis;
- the shaped coil was heat-treated using a hot-air heater in order to stabilize the geometry and preserve the imposed configuration.

After pre-shaping the braided sleeve to the desired geometry, a short tube was inserted into the proximal end of the sleeve to provide a pneumatic interface. Inside the sleeve, a small elastic balloon was positioned so as to act as an internal inflatable chamber. The tube was then connected to a DC-powered pneumatic source (pump/valve), enabling controlled pressurization of the balloon. Upon inflation, the balloon expanded within the sleeve and induced an axial elongation of the structure, increasing the overall extension of the internal element.

The resulting specimen (Figure 3.10) was connected to a pneumatic supply line and tested to qualitatively assess (i) shape stability under repeated pressurization cycles and (ii) feasibility for McKibben-type extension.

Figura 3.10: Bellow-shaped braided specimen used for preliminary McKibben-type extension tests.

Figure 3.11 reports the instrumentation used in the preliminary pneumatic tests. A diaphragm pump was used as pneumatic source, while an electro-pneumatic element (valve/regulator) modulated the delivered actuation level to the specimen. The command was provided as a DC voltage. In this work, V_{set} indicates the voltage set on the bench power supply, whereas V_{meas} denotes the voltage measured with a multimeter at the input of the electro-pneumatic component.

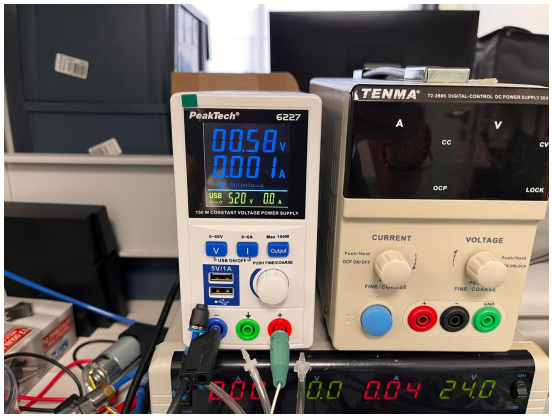

(a) Bench DC power supplies used to generate the control voltage for the electro-pneumatic element.

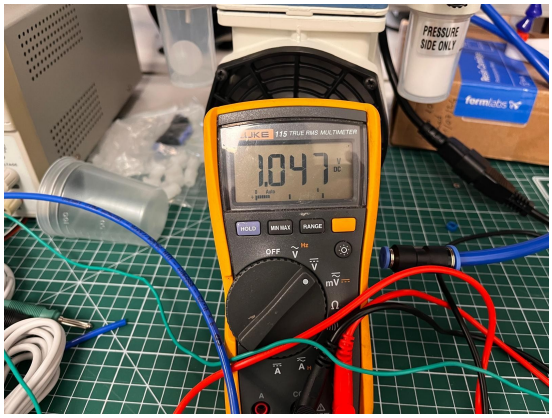

(b) Diaphragm pump (pneumatic source) and digital multimeter used to monitor the applied voltage.

Figura 3.11: Experimental setup instrumentation for preliminary pneumatic tests.

During the experiment, the specimen was placed on a planar surface with a regular grid pattern, used as a visual reference for length measurements. For each voltage step, the system was allowed to reach a quasi-steady configuration and the axial position of the distal end was recorded from the grid. Table 3.1 summarizes the recorded distal-end positions as a function of the electrical command.

Tabella 3.1: Preliminary axial extension of the braided specimen as a function of the applied control voltage. Distal-end position was estimated from the cutting-mat reference scale.

V_{set} [V]	V_{meas} [V]	Position [cm]	ΔPosition [cm]
0.00	–	65	0
0.58	1.047	67	2
1.34	1.487	$\sim$69	$\sim$4
1.44	1.520	70	5
1.70	1.604	71	6

Representative configurations during extension are reported in Figure 3.12, showing the progressive increase in axial length as the actuation command increased.

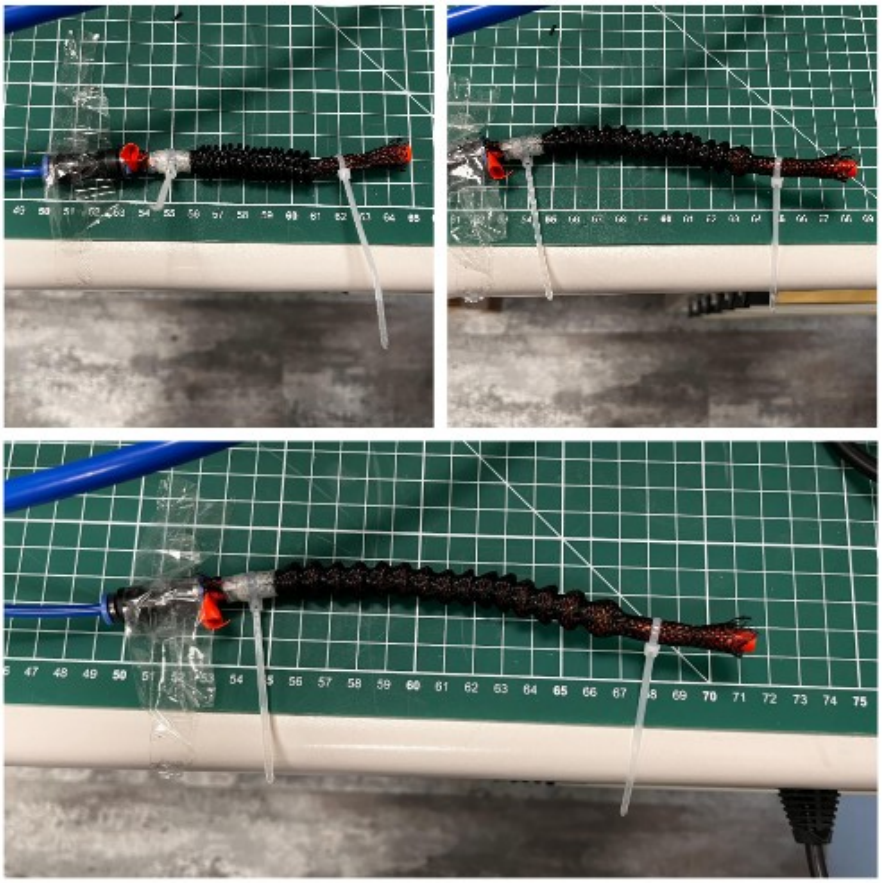

Figura 3.12: Representative extension configurations of the bellow-shaped braided specimen under increasing actuation command. The distal-end position was read from the cutting-mat scale.

Overall, the modified braided specimen exhibited a clear extensible response as the electrical command increased, with an estimated distal-end displacement of approximately 6 cm over the investigated range. These preliminary results support the feasibility of using the reshaped braided coil as a reinforcement for McKibben-like actuation.

3.5 First model

Based on the silicone-coated braided sleeve's behaviour under tension and compression, I developed the first robotic arm prototype incorporating this reinforcement. A practical challenge emerged when preparing a 27 cm-long coated element: due to its slender geometry, obtaining a uniform and bubble-free silicone layer by manual coating is difficult. In the initial approach, a metal tube (diameter $\approx$ 3.25 mm)

was inserted inside the braided sleeve to provide support and alignment, and the sleeve was then manually coated with silicone along its length. Ecoflex 00-10, which provided the best results in the preliminary tests, was particularly suitable for this step because its higher viscosity reduced uncontrolled flow and helped maintain a more consistent coating thickness.

Thanks to this property, I decided not to use any external support. Instead, I held the silicone-coated fiber vertically and manually adjusted its position as the silicone slowly flowed downward. By carefully repeating this process for about 30 to 40 minutes, I obtained a nearly perfect silicone coating. This result was only possible thanks to the high viscosity of Ecoflex 10.

Once the silicone had fully cured (4 hours), the nylon fishing line was routed through the braided sleeve. To anchor the tendon, a small 3D-printed cylindrical support with a flared base was designed (Fig. 3.13). The part includes a through-hole (0.8 mm) to guide the fishing line. After threading the line through the support, a stopper knot was tied at the end, mechanically locking the tendon within the printed component. This anchoring strategy prevents slippage during actuation and enables reliable bending of the arm when the tendon is pulled, as the tensile load is effectively transferred to the embedded internal element.

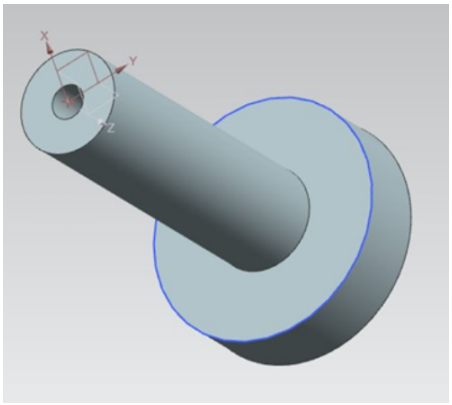

Figura 3.13: support for the fiber

At this point, I inserted the fiber with the wire into the mold (Figure 3.14), closed the mold, and poured in Ecoflex 20 silicone (which is commonly used in soft robotic arms).

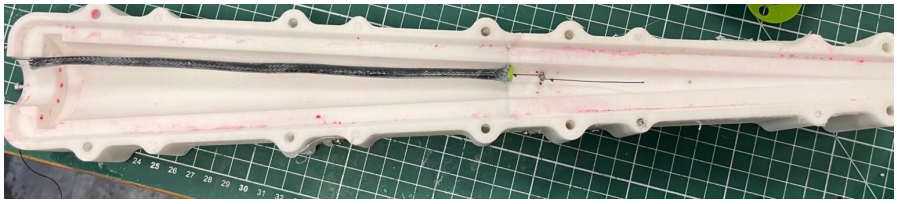

Figura 3.14: Mold with the fiber insert

After the silicone had fully cured, I removed the arm from the mold; the result is shown in Figure 3.15.

Figura 3.15: Firs octopus arm

3.6 Second model

After preliminary tests on the pneumatic part were performed, the design process was redirected towards the original concept. This shift was made possible thanks to the collaboration with a company that provided materials with geometries and designs similar to those previously used, but with smaller dimensions and therefore more suitable for the purpose of the project. Specifically, two types of nylon fiber were identified:

- a nylon fiber with the same coil-like geometry used in the first design phase,
- the same nylon fiber coated with a silicone layer, in order to improve mechanical resistance and durability.

The main idea is to build a soft robotic arm by exploiting the complementary properties of these two materials. Inside the structure, a fishing line is placed which, is allowed to protrude outside the arm and is manipulated externally. By pulling the fishing line, the arm bends, thus enabling controlled motion and allowing the movement principle of the prototype to be tested and validated. The combined use of nylon and silicone therefore allows the development of a flexible yet resistant design, capable of mimicking, although in a simplified manner, the behavior of an octopus tentacle, while also providing a solid experimental basis for the subsequent development of control strategies.

As a first experimental step, the white nylon fiber was tested by constructing a prototype of the soft robotic arm. In this configuration, two fibers were employed: the first with a standard length, ending at the same position used in previous designs, and the second slightly longer, extending deeper into the structure. This design choice was made in order to observe and compare the behavior of the arm tip as a function of the different fiber lengths. Figure 3.16

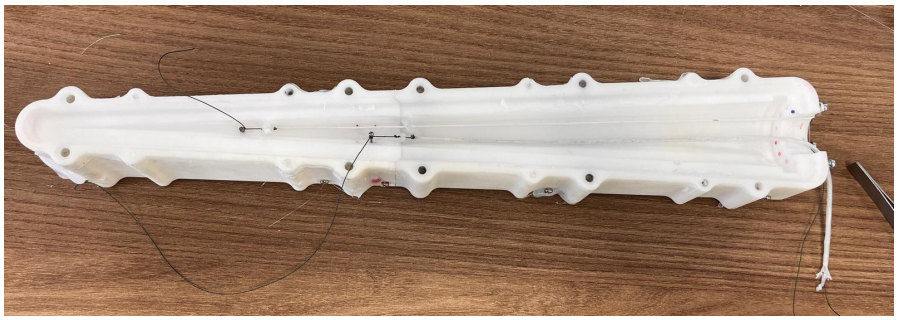

Figura 3.16: Mold of the octopus-inspired soft arm with two nylon fibers of different lengths positioned prior to silicone casting.

Subsequently, as illustrated in the Figure 3.17, small supports were added at the fiber terminations and secured with knots, in order to guarantee proper anchoring and prevent fiber slippage during actuation. With this arrangement, the external traction applied to the fibers enables the arm to bend smoothly and consistently, without stability losses or undesired detachment.

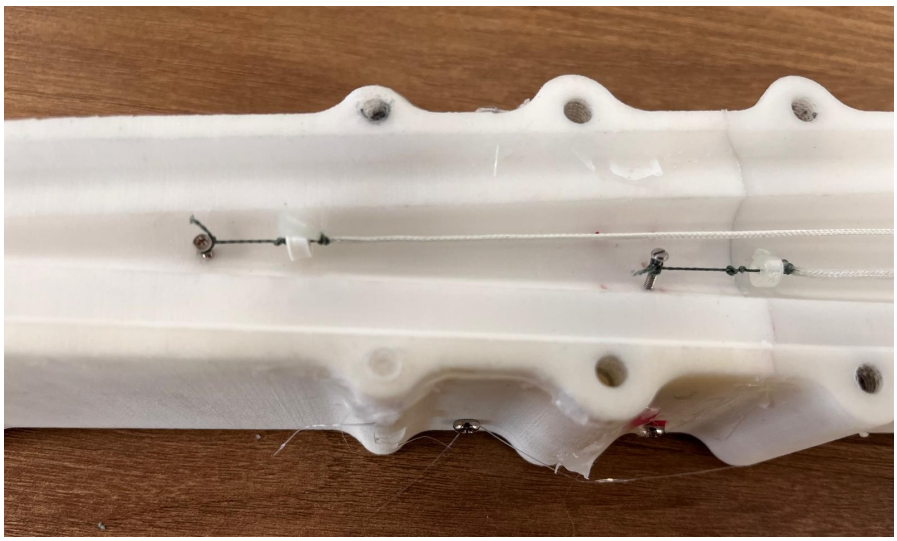

Figura 3.17: Detail of the tendon anchoring and termination system used in the prototype.

3.7 Third model

As a next step, a fourth prototype of the octopus-inspired arm was developed by modifying the internal reinforcement material while preserving the external geometry of the arm. The objective of this design iteration was to investigate the effect of a commercially manufactured reinforcement with improved geometric regularity and reduced diameter, compared to the manually fabricated silicone-coated braided coil adopted in previous designs.

3.7.1 Materials and structural configuration

The reinforcement adopted in this design consists of a silicone-rubber-coated braided fiberglass sleeve. The sleeve is composed of an internal woven fiberglass braid, which provides high tensile strength and dimensional stability, uniformly coated with a thin layer of silicone rubber.

The braided fiberglass core ensures mechanical robustness and resistance to axial loads, while the external silicone coating enhances flexibility and compliance. In addition, the silicone layer improves adhesion and frictional interaction with the surrounding elastomeric matrix of the arm, reducing relative sliding during deformation and actuation.

Compared to the previously used hand-coated braided reinforcement, this commercially available sleeve offers a more uniform diameter, a regular braid pattern, and improved manufacturing repeatability. The reduced diameter of the sleeve allowed easier integration within the arm cross-section while maintaining sufficient stiffness for force transmission. For these reasons, this material was selected as an alternative reinforcement solution aimed at improving structural consistency and repeatability without compromising the compliant behavior required for soft robotic applications.

3.7.2 Integration within the arm

A single silicone-coated braided sleeve was inserted along the length of the arm, extending from the base up to approximately 6 cm from the distal end. A fishing line was routed inside the sleeve and used as a tendon for actuation: when pulled from outside the arm, it generates bending by applying tensile load along the reinforced path.

The braided sleeve and the fishing line were positioned within the arm following the same internal configuration adopted in the previous design based on the silicone-coated fiber. The terminal support previously used in earlier iterations was retained to ensure reliable anchoring of both the reinforcement and the tendon during operation.

The overall external shape and dimensions of the arm remained unchanged with respect to previous prototypes; the modifications introduced in this design were limited exclusively to the characteristics of the internal reinforcement and the actuation layout.

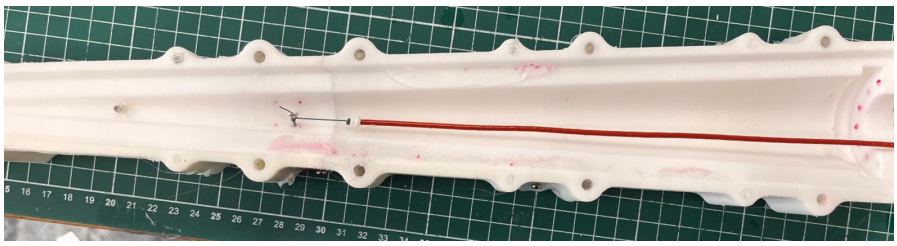

Figura 3.18: Fourth design prototype integrating a silicone-rubber-coated braided fiberglass sleeve as internal reinforcement.

3.7.3 Design considerations

The use of a commercially manufactured silicone-coated braided sleeve was motivated by the need for improved geometric precision and repeatability compared to manually fabricated reinforcements. While the functional concept remains similar to that of the silicone-coated braided coil described in earlier sections, the present solution reduces fabrication variability and provides a more controlled structural response.

This design represents an intermediate step toward more reliable and scalable fabrication of soft robotic arms, maintaining bio-inspired compliance while improving robustness and consistency of the internal reinforcement.

3.8 Fourth model

In a later stage of the design, I investigated the use of an internal skeleton inspired by the spiral robotic structure (Fig. 3.19) presented in the literature [49].

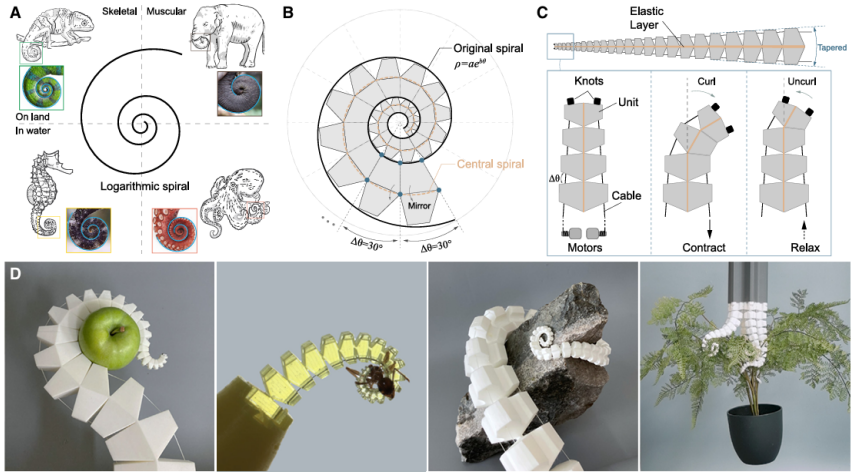

Figura 3.19: Bioinspiration and design principle of spiral robots [49].

Figure 3.20 reports the reference SpiRobs geometry reproduced in Siemens NX and used as an initial baseline for this study. Since SpiRobs was originally conceived as an autonomous robot rather than an insertable reinforcement, I first fabricated a reduced prototype by resin printing the reference geometry. The printed part was placed in a mold and cast in silicone to qualitatively evaluate feasibility aspects, namely resin–silicone adhesion and the resulting bending behaviour (Fig. 3.21).

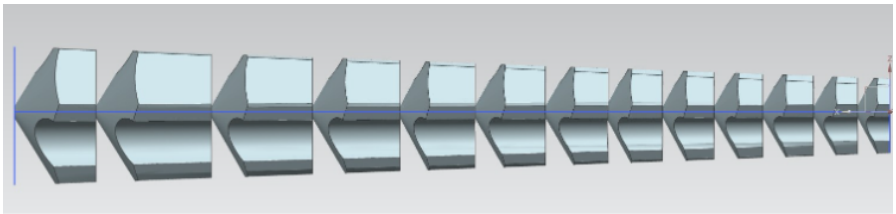

Figura 3.20: Reference CAD geometry of the SpiRobs-inspired spiral structure reproduced in Siemens NX and used as the initial baseline.

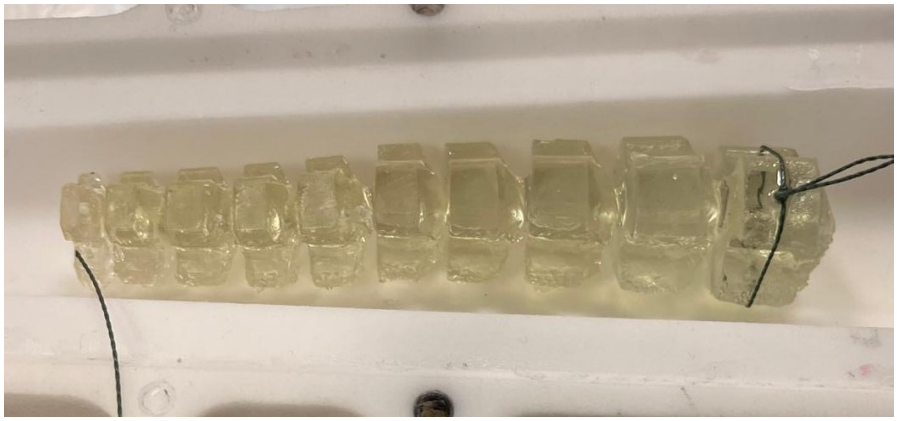

Figura 3.21: Resin-printed prototype of the reference SpiRobs-inspired geometry, cast in silicone to qualitatively assess resin–silicone adhesion and bending behaviour.

After resin-printing the skeleton and analysing its qualitative kinematics, we verified the material compatibility and manufacturability of the resin–silicone pairing at the target scale. To this end, the skeleton was placed inside a dedicated mold and over-moulded to fabricate a silicone arm embedding the structure. This prototype was not intended to be functional or actuated; its sole purpose was to assess:

- whether the resin cured and bonded properly within silicone without interfacial defects,
- whether an internal skeleton embedded in the silicone body could support and guide the bending motion without constraining it

During assembly and silicone casting, the skeleton was successfully integrated, confirming compatibility between resin and silicone: the silicone cured properly around the resin without noticeable interfacial issues. However, initial manual bending tests revealed that some regions of the skeleton were relatively thick, generating significant internal friction and increasing resistance to bending. Additionally, careful attention during casting was required to avoid air bubbles and ensure correct centering of the skeleton, in order to achieve uniform and repeatable bending.

Based on these observations, the geometry was re-parameterized to operate as an internal skeleton embedded within a silicone arm, while preserving the key spiral-inspired feature of SpiRobs designs, namely a graded, self-similar discretization that promotes increasing curvature capability toward the distal end.

To provide an immediate visual overview of the graded discretization along the arm, Fig. 3.22 reports a clean side view of the skeleton, highlighting the progressive reduction of feature size toward the distal end.

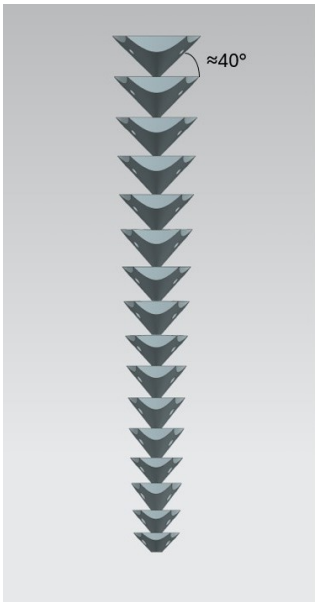

Figura 3.22: Aligned side view of the internal skeleton showing the graded discretization into modular units and the progressive reduction in size and spacing toward the distal end. The inter-unit angle ($\theta \approx 40°$) is also highlighted.

3.8.1 Geometrical re-parameterization inspired by SpiRobs

The redesign aimed at enabling tendon-driven actuation while preserving the spiral-inspired graded architecture. In SpiRobs, the spiral/logarithmic construction leads to a self-similar structure where local geometry is preserved while scale changes progressively along the body [49]. In the present work, rather than explicitly generating a spiral curve, the same principle was captured through a graded discretization along the arm longitudinal axis.

Each modular unit consists of a toothed profile with three symmetrically distributed longitudinal holes that define tendon routing and preserve cross-sectional symmetry. The unit *shape* is kept constant, while its overall size and the axial spacing between consecutive units are progressively scaled from proximal to distal regions.

A perspective view of the skeleton is reported in Fig. 3.23b to clarify the graded modular construction prior to introducing the scaling laws.

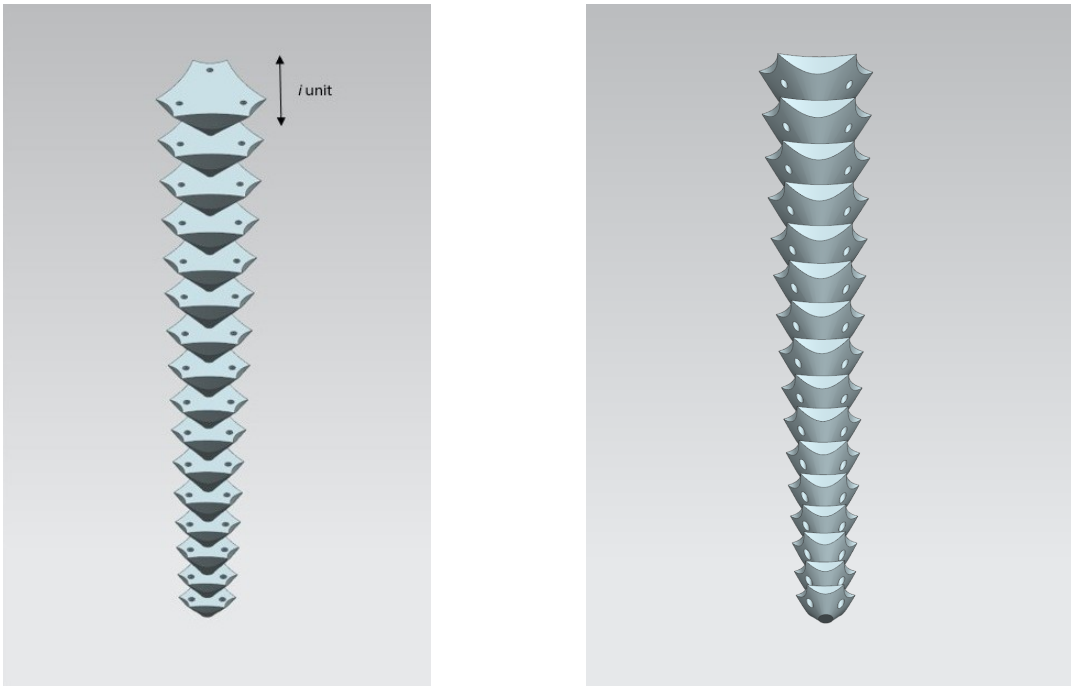

(a) Aligned view showing the combined reduction in unit size and axial spacing from proximal to distal regions.

(b) Perspective view showing the graded modular architecture along the longitudinal axis.

Figura 3.23: Graded internal skeleton architecture. (a) Aligned view highlighting the progressive reduction in unit size and spacing. (b) Perspective view illustrating the modular arrangement along the longitudinal axis.

The skeleton was decomposed into a sequence of N stacked modular units indexed by $i \in \{0, \ldots, N-1\}$. A characteristic size parameter s_i (e.g., maximum unit width in top view) was defined for each unit and described through an exponential scaling law:

$$s_i = s_0\, q^{\,i}, \qquad 0 < q < 1, \tag{3.1}$$

where s_0 is the size of the proximal unit and q is the constant reduction factor controlling the degree of downsizing toward the distal region. Once s_0, s_{N-1}, and N are measured in NX, the scaling factor can be obtained as:

$$q = \left(\frac{s_{N-1}}{s_0}\right)^{\frac{1}{N-1}}. \tag{3.2}$$

Similarly, the axial spacing (pitch) between consecutive units was re-parameterized to increase unit density toward the distal end:

$$p_i = p_0\, q_p^{\,i}, \qquad 0 < q_p < 1, \tag{3.3}$$

where p_i denotes the spacing between unit i and unit $i+1$. From the measured values p_0 and p_{N-1}, the pitch reduction factor is:

$$q_p = \left(\frac{p_{N-1}}{p_0} \right)^{\frac{1}{N-1}}. \tag{3.4}$$

This combined reduction in unit size and spacing increases distal compliance and enables smaller achievable bending radii, thus promoting curling behaviour under tendon actuation. An aligned view illustrating the effect of the graded scaling is shown in Fig. 3.23a.

3.8.2 Structural modifications for tendon actuation and manufacturability

After the initial experiments, the internal skeleton was redesigned to enable tendon-driven actuation and improve flexibility. The design of the cross-sectional geometry was therefore driven by the need to accommodate three tendons, leading to a three-holes configuration in which each holes hosts one tendon channel. As shown in Fig. 3.24, the tendon channels are symmetrically distributed and positioned close to the outer boundary to increase the actuation moment arm and enhance bending performance. To ensure geometric consistency, the unit shape was constructed starting from a circular reference by defining three radial directions equally spaced by 120°, which were used to position the tendon channels and generate the external profile.

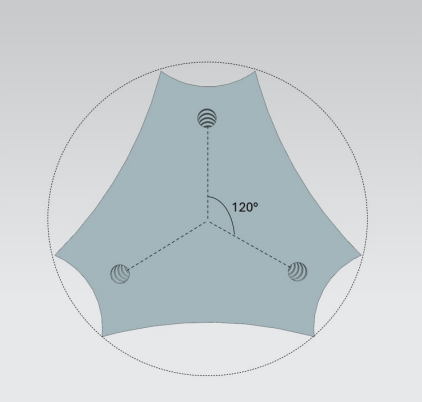

Figura 3.24: Top view of a single modular unit showing the three symmetrically distributed tendon channels and the three-lobed geometry used for tendon routing.

To address the internal friction and local stiffness observed in the first prototype, unit size and thickness were reduced, sharp corners were filleted, and the spacing between segments was re-parameterized according to the graded law described

above. In addition, the thickness of the "teeth" was reduced and the inter-unit angle was set to approximately 40°, limiting resin–silicone rubbing, facilitating smoother curling, and reducing wear.

These modifications also improved manufacturability during casting by mitigating air entrapment and alignment issues. The resulting redesigned structure is shown in Fig. 3.25, where the combined effect of geometric smoothing, downsizing, and graded spacing can be observed.

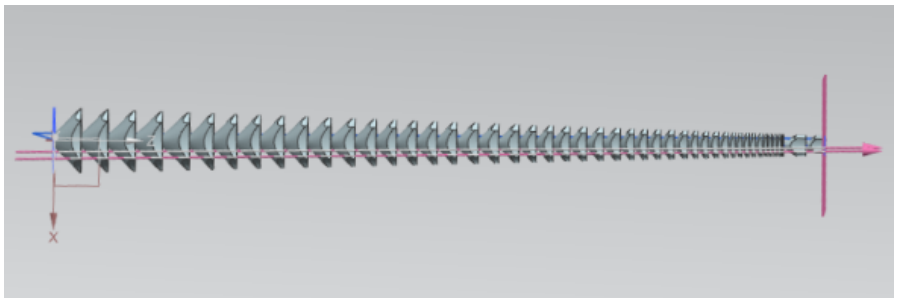

Figura 3.25: Redesigned internal skeleton in Siemens NX: three edge tendon channels, downsized units with filleted geometry, and a pronounced distal spacing gradient.

In addition to the overall downsizing of the units, the spacing gradient was made more pronounced, starting at approximately 1.5 mm and decreasing to about 0.4 mm toward the distal end. This refinement was essential to increase bending compliance and achieve smoother, more controlled curling under tendon actuation.

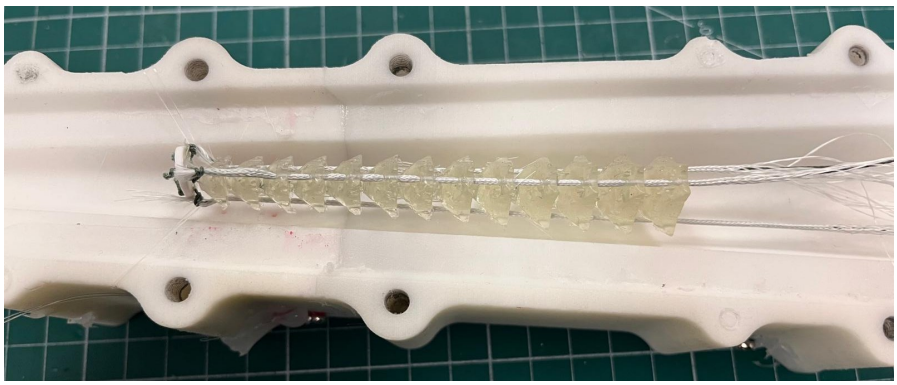

Figura 3.26: Small skeleton on the mold

3.8.3 Reduced-scale prototype and qualitative assessment

To characterise the behaviour at the distal section, a reduced-scale prototype of the arm was fabricated. The model was designed in Siemens NX and printed on

a Prusa resin printer. The resin components were made slightly thinner than the surrounding arm (5 mm vs. 8 mm) to ensure a sufficient silicone cover after casting, improving adhesion, elasticity, and structural integrity.

Along the skeleton, three longitudinal holes housed a white flexible sleeve containing a nylon fishing line. The sleeve prevented the line from cutting into the resin under tension. At the distal end, a disk-shaped support with three holes secured the cables and prevented slippage, thus preserving system stability and avoiding rework.

(a) Reduced-scale silicone arm used to assess distal-section behaviour.

(b) Bending sequence showing flexibility and silicone distribution during deformation.

Figura 3.27: Experimental evaluation of the reduced-scale arm. (a) Prototype used for distal behaviour assessment. (b) Bending sequence illustrating deformation under actuation.

Preliminary manual manipulation suggested a favourable qualitative behaviour: bending appeared smoother and more uniform, with a consistent elastic response. Although no quantitative evaluation was performed at this stage, the graded architecture seemed to facilitate curling during tendon pulling and to improve controllability by hand. Based on these initial impressions, this skeleton was selected as the final design, extending along the entire arm up to 10 mm from the tip.

3.9 Final design

The final design focused on the development of a dedicated distal section, where strong geometric and dimensional constraints prevented the adoption of the same multi-tendon architecture used in the central portion of the arm. In particular, the reduced diameter of the octopus arm tip made it impractical to route three independent tendon channels. As a result, the terminal segment was intentionally

designed to accommodate a single tendon only, leading to an asymmetric yet controlled bending behaviour.

The overall arm configuration builds directly upon the fifth design presented in the previous section. The internal skeleton geometry developed for that prototype was retained along the main body of the arm, as it demonstrated satisfactory mechanical performance in terms of compliance, robustness, and reliable tendon routing. Consequently, the design effort for the final iteration was concentrated on the distal region, while keeping the rest of the structure unchanged in order to limit the number of variables introduced between successive prototypes.

3.9.1 Single-tendon distal terminal geometry

The distal terminal segment was designed as a tooth-like structure mechanically coupled to the end of the internal skeleton. Unlike a purely passive terminal element, this segment is *tendon-driven*: a nylon fishing line runs inside a dedicated channel and, when tension is applied, the tip bends predominantly toward the tendon side. The tendon channel was designed with a diameter of 0.8 mm, sufficient to route a single fishing line while preserving structural integrity at this scale.

The geometry consists of a sequence of discrete teeth arranged along the longitudinal axis. Both the characteristic size of the teeth and the axial spacing between consecutive teeth decrease progressively toward the distal end. In other words, the terminal geometry follows a graded discretization, where smaller features and denser spacing are found near the tip. This gradual reduction was introduced to locally decrease bending stiffness and facilitate curling during tendon pulling, promoting smoother deformation and reducing the likelihood of abrupt kinks.

Importantly, the shape of each tooth remains geometrically similar along the sequence Fig. 3.28., while its scale and spacing are progressively reduced. This approach captures the same functional principle observed in spiral-inspired robotic structures, such as SpiRobs, where self-similarity and scale variation along the body lead to enhanced distal curvature. In the present design, this effect is achieved without explicitly generating a spiral geometry, but rather through a one-dimensional graded discretization compatible with the severe dimensional constraints at the arm tip.

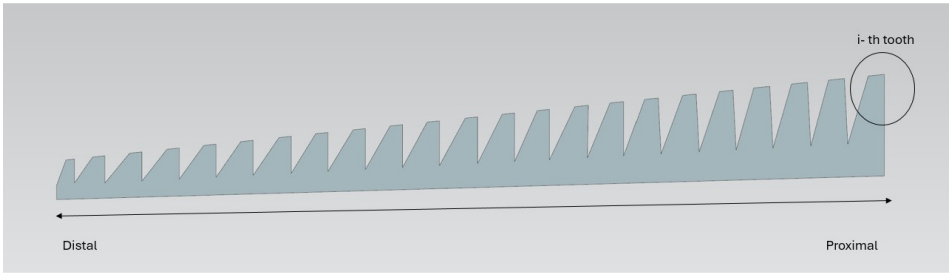

Figura 3.28: Overview of the final distal terminal geometry integrated with the internal skeleton. The tooth-like structure follows a graded discretization with decreasing feature size and spacing toward the distal end.

A detailed view of the terminal geometry is shown in Fig. 3.29. The progressive reduction in tooth size and spacing leads to a compliant region that naturally assists curling under tendon tension, despite the absence of independent actuators embedded in the distal section.

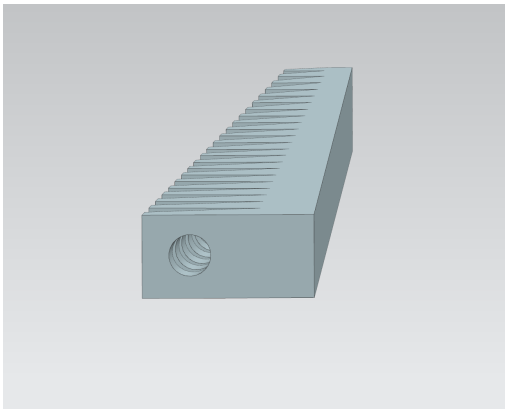

Figura 3.29: Detail of the tooth-like distal segment. A single tendon channel (0.8 mm diameter) routes the fishing line; the graded reduction in tooth size and spacing increases distal compliance and assists curling during tendon pulling.

This geometric solution was motivated by qualitative observations of octopus arm behaviour, where active control appears to be concentrated in a limited portion of the limb, while the distal end often remains curled. By exploiting a graded,

tooth-based geometry together with a single tendon, the final design supports a controlled curling response at the tip while respecting the dimensional constraints of the distal region.

3.9.2 Assembly and tendon anchoring

Figure 3.30 shows the internal layout of the final prototype before silicone casting. The main body retains the previously developed graded internal skeleton, while the tooth-like distal component is coupled to its end to form the terminal section. This modular approach ensured continuity between the reinforced central region and the redesigned tip, while allowing the distal geometry to be modified without altering the rest of the skeleton.

The nylon fishing line is routed through the distal tip via the internal channel and guided by a protective sleeve to improve alignment and mitigate local abrasion during tensioning. At the proximal end, the tendon is secured to a dedicated anchoring support , which provides a stable attachment point and helps maintain repeatable tendon positioning during casting and subsequent operation. After positioning the skeleton, distal tip, tendon sleeve, and anchoring support, the mould was closed and silicone was poured , resulting in a monolithic soft arm embedding the complete internal architecture.

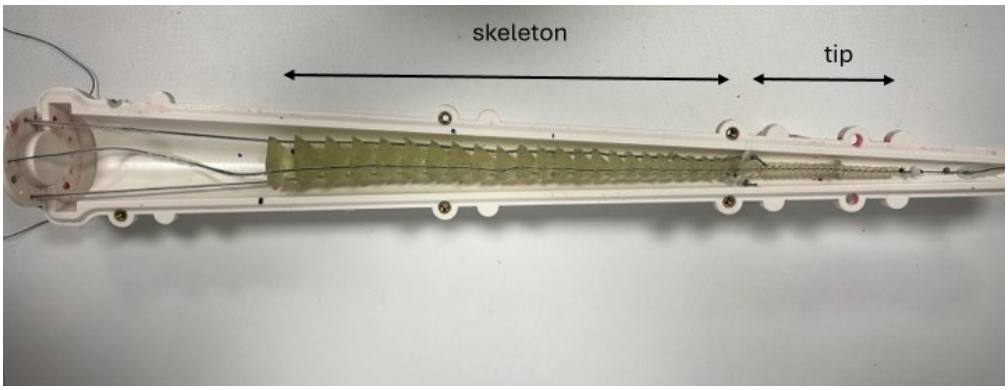

Figura 3.30: Internal assembly of the final prototype before silicone casting: the previously developed internal skeleton is integrated with the tooth-like distal tip, while the nylon fishing line is routed through a protective sleeve and anchored proximally via a dedicated support.

Overall, the final design combines the validated internal skeleton developed in the fifth design with a dedicated single-tendon distal geometry tailored to morphological and manufacturing constraints. This approach allowed incremental refinement of the arm architecture while preserving a clear link between geometry, actuation strategy, and expected tendon-driven deformation behaviour.

Capitolo 4

Experimental results on design

4.1 Introduction

4.2 Experimental Evaluation

This section presents the experimental evaluation of the designed soft robotic arm prototypes. The aim of these experiments was to analyse the deformation behaviour and bending actuation of the arm when actuated through a tendon-driven mechanism.

Several arm prototypes with different internal structural configurations were tested in order to evaluate how the internal reinforcement affects the bending behaviour of the arm. In particular, three configurations were investigated: a white-wire reinforced arm, a braided sleeve reinforced arm, and a red-wire reinforced arm.

The experiments were designed to measure the relationship between the motor actuation input and the resulting bending angle of the arm. The obtained results allow a quantitative comparison of the different internal structures and provide insights into their influence on the mechanical response of the soft robotic arm.

4.3 Methods

4.3.1 Experimental Setup

The actuation system consists of two Dynamixel servo motors (Dynamixel XM430-W210-R), but in the test it's just one needed, which are used to generate the pulling

forces required to bend the arm.

Figura 4.1: Dynamixel XM430-W210-R servo motors used for tendon actuation.

The motors are mounted on a rigid structure placed above the arm support. Each motor is connected to a tendon of each arms . The tendons are routed from the base of the arm to the motors and wrapped around the motor pulleys.

4.3.2 Tendon-Driven Actuation System

The soft arm is actuated through a tendon-driven mechanism. The tendons pass through the base of the arm and are guided toward the motors positioned above the structure. The tendons are wrapped around the motor pulleys so that when the motors rotate, the tendons are pulled, generating tension along the arm and producing bending deformation.

The rotation of the motors therefore results in a linear displacement of the tendons. By controlling the motor rotation, different levels of tendon displacement can be applied, which in turn produce different bending configurations of the soft arm. This allows the deformation behaviour of the arm to be analysed as a function of the motor input.

4.3.3 Experimental Configuration

The complete experimental setup is shown in Fig. 4.3. The arm is mounted vertically and clamped to ensure a fixed boundary condition at the base. This configuration allows the arm to deform freely while the tendons are actuated by the motors.

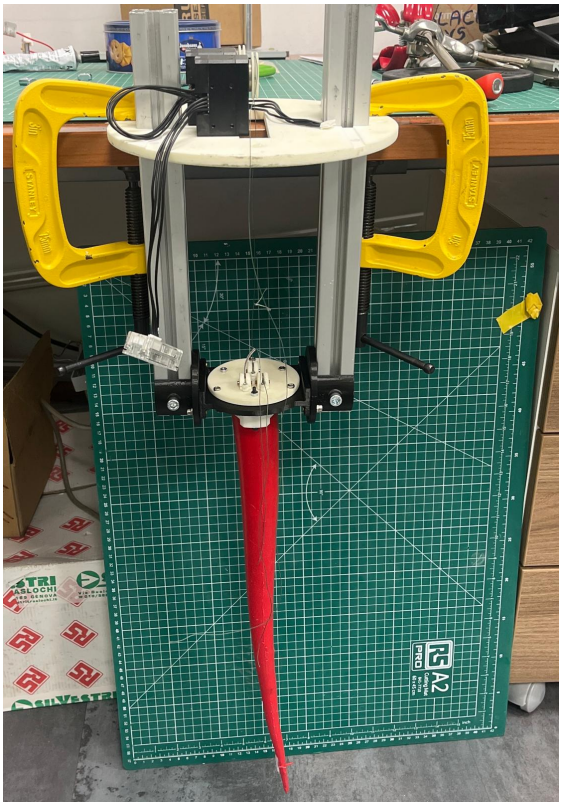

Figura 4.2: Experimental setup used to actuate the soft robotic arm through a tendon-driven mechanism.

During the experiments, the motors were commanded to rotate by a predefined amount, producing a controlled displacement of the tendons and therefore bending the arm.

4.3.4 Motion Tracking and Data Processing

The deformation of the arm during the experiments was recorded using video acquisition. The recorded videos were analysed using the motion analysis software Kinovea, which allowed tracking the position of specific points on the arm, such as the base reference point and the tip of the arm.

During the experiment, the arm was initially positioned in its straight configuration (Fig. 4.3), corresponding to a motor input value equal to zero. This configuration was used as the reference configuration for the bending angle computation. The base of the arm was fixed to the support structure, and a reference point located at the base was used as the origin for the geometric measurements.

The actuation was applied by progressively increasing the motor command using the Dynamixel Wizard interface. Different motor input values were tested in order

to generate increasing tendon tension and therefore increasing arm deformation. In particular, the following actuation values were applied during the test: 2000, 3000, 4000, 5000, and 7000 motor units.

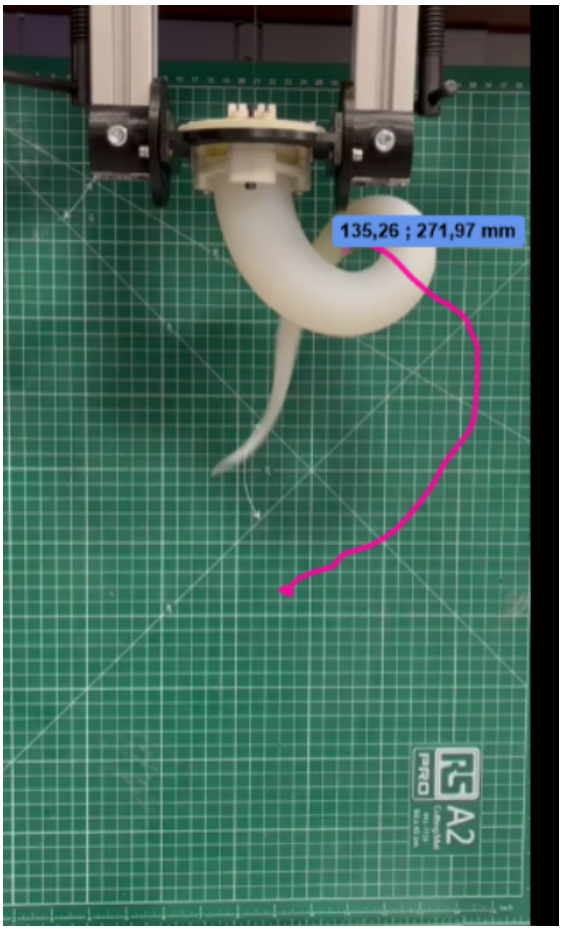

Figura 4.3: Example of tracking with Kinovea

The coordinates extracted from Kinovea were then processed in MATLAB to compute the bending angle of the arm during the actuation.

4.3.5 Bending Angle Computation

The bending behaviour of the soft robotic arm was evaluated by analysing the recorded videos of the experimental tests. The videos were processed using the motion analysis software Kinovea, which allows tracking the position of selected points along the structure.

Two points were defined on the arm for the analysis: a reference point located at the base of the arm and a point located at the tip of the arm. The position

of the tip was tracked in two different configurations of the arm: the initial straight configuration and the actuated (bent) configuration obtained during tendon actuation.

By marking these points in the video frames, the corresponding coordinates were extracted. The bending angle of the arm was then computed by comparing the direction of the arm in the straight configuration with the direction of the arm in the bent configuration.

Let $refpoint$ be the point located at the base of the arm, p_1 the position of the tip in the straight configuration, and p_2 the position of the tip in the bent configuration. Two vectors describing the orientation of the arm in the two configurations can therefore be defined as

$$v_1 = p_1 - refpoint \tag{4.1}$$

$$v_2 = p_2 - refpoint \tag{4.2}$$

The bending angle θ between the two vectors was computed using the following formulation

$$\theta = \text{rad2deg}\left(\text{atan2}\left(\|v_1 \times v_2\|, v_1 \cdot v_2\right)\right) \tag{4.3}$$

where θ represents the bending angle between the initial straight configuration of the arm and the actuated configuration. The extracted coordinates were processed using MATLAB in order to compute the bending angle for the different actuation levels applied during the experiments.

4.4 Results

4.4.1 White Wire Arm Test

The results of the White Wire Arm Test shows a progressive increase of the bending angle as the motor input increases. For example, when the motor command was set to 2000 units, the arm exhibited a moderate bending configuration with a measured bending angle of approximately 9.83°. Increasing the motor input to 3000 resulted in a larger deformation, producing a bending angle of approximately 25.78°. Further increases of the motor command generated more pronounced curvature of the arm, reaching approximately 42.26° at 4000 motor units, 57.27° at 5000 motor units, and approximately 74.05° at 7000 motor units.

These results confirm that the tendon-driven actuation system is capable of producing controlled and progressive bending of the soft robotic arm. The relationship between motor input and bending angle demonstrates the ability of the system to generate different arm configurations through tendon tension control.

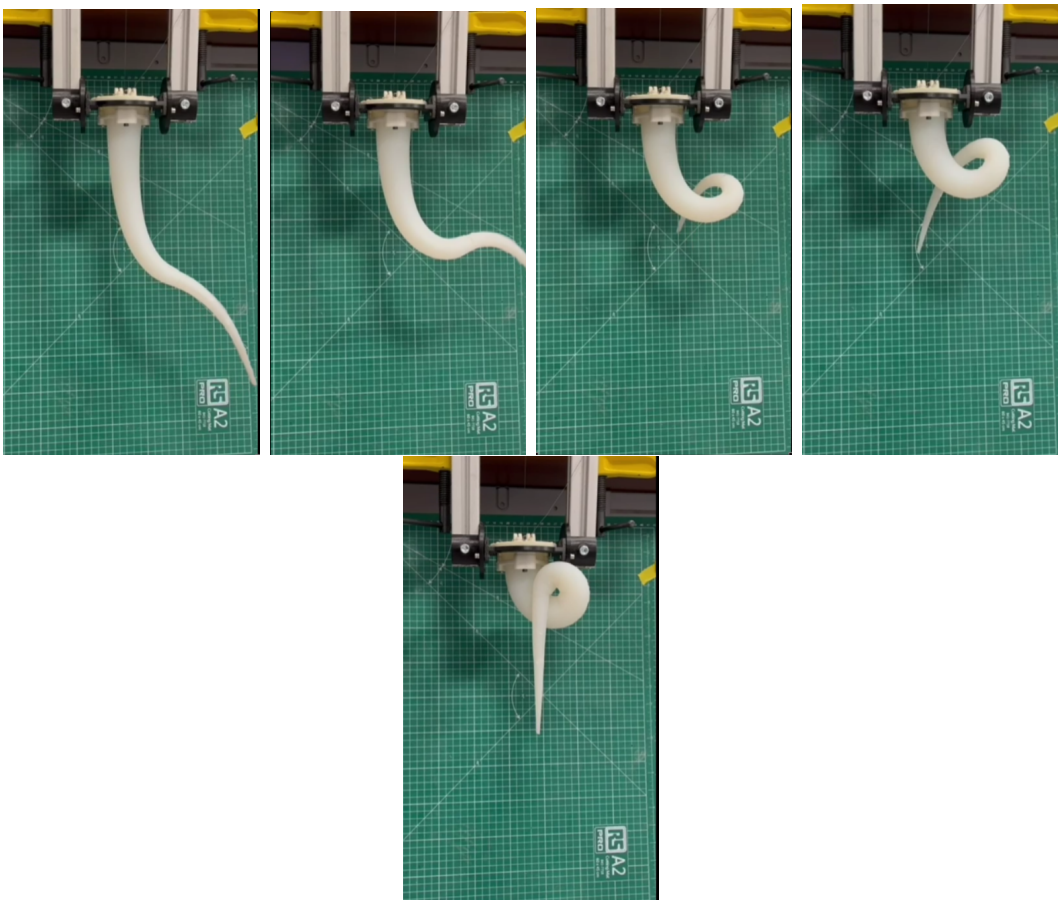

Figura 4.4: Deformation of the white-wire soft arm prototype under different motor actuation levels. From left to right: 2000, 3000, 4000 and 7000 Dynamixel motor units.

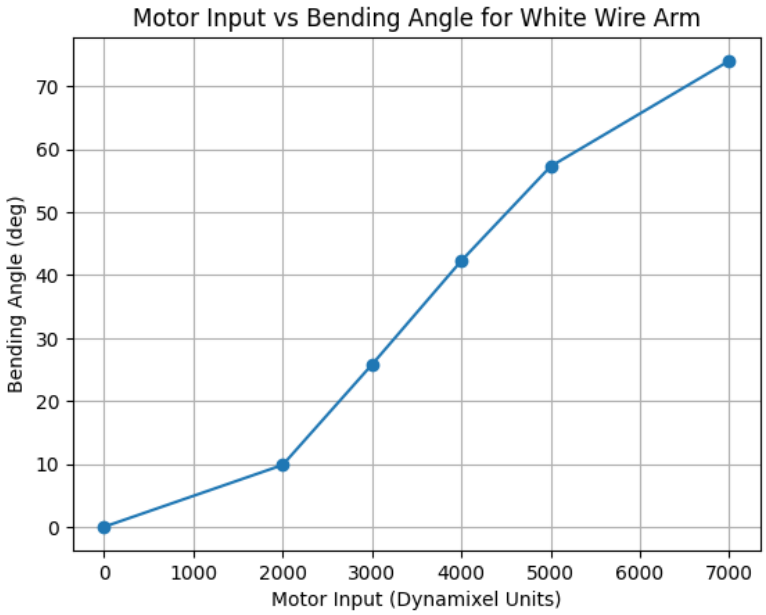

Figura 4.5: Relationship between the Dynamixel motor input and the resulting bending angle of the white-wire soft arm prototype.

4.4.2 Braided Sleeve Arm Test

A second experimental campaign was conducted using a soft arm prototype reinforced with a braided sleeve structure covered with silicone. The resulting bending angles obtained from the experiments are reported below:

- 2000 motor units: 18.03°
- 3000 motor units: 32.46°
- 4000 motor units: 45.85°
- 5000 motor units: 50.90°
- 7000 motor units: 62.57°

The results show that the braided sleeve structure produces a progressive bending behaviour as the tendon actuation increases. However, compared to the previous white-wire configuration, the arm exhibits a different stiffness profile, with the deformation increasing more gradually for higher motor inputs.

This behaviour can be attributed to the mechanical constraints introduced by the braided reinforcement, which partially limits the radial expansion of the silicone body and influences the resulting bending mechanics of the arm.

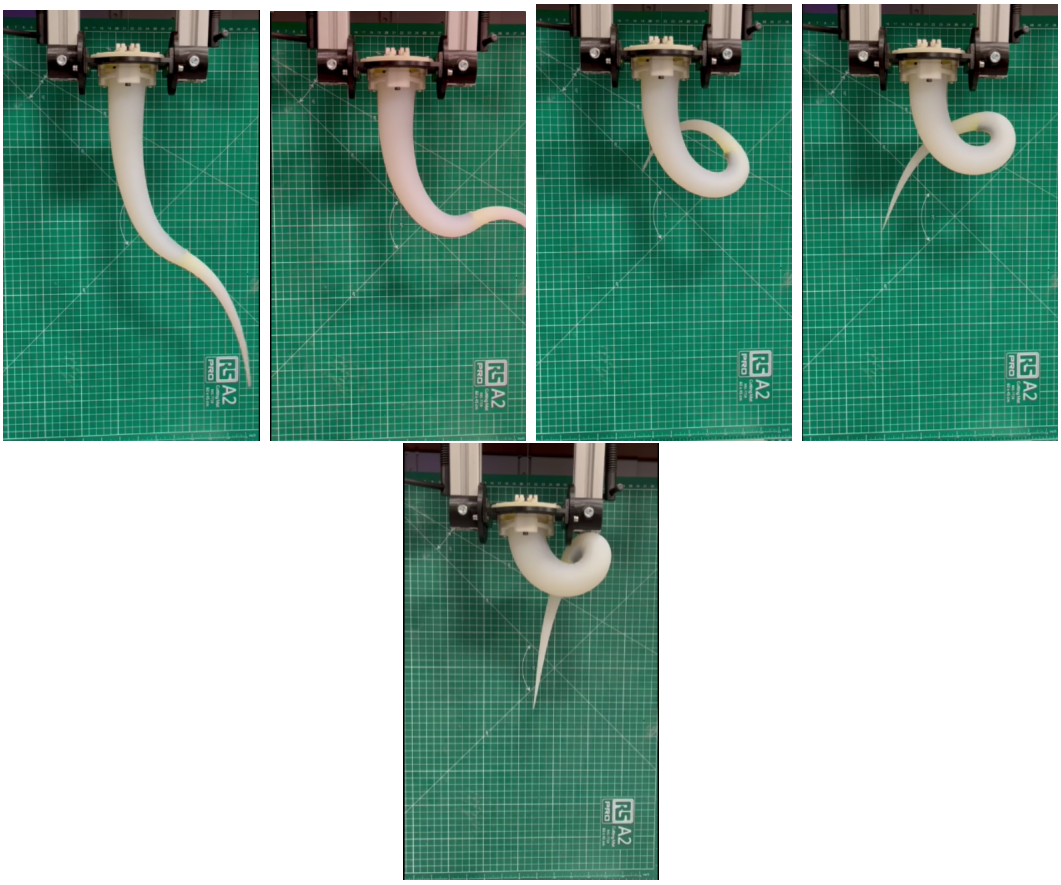

Figura 4.6: Deformation of the white-wire soft arm prototype under different motor actuation levels. From left to right: 2000, 3000, 4000 and 7000 Dynamixel motor units.

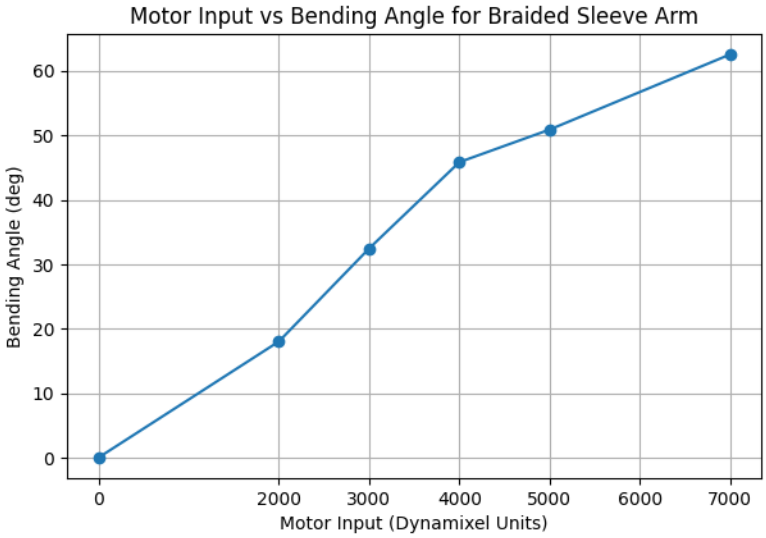

Figura 4.7: Relationship between the Dynamixel motor input and the resulting bending angle of the white-wire soft arm prototype.

4.4.3 Red Wire Arm Test

A third experimental test was performed using a soft robotic arm prototype reinforced with red internal wires embedded in the silicone body.

The bending angles measured during the experiment are reported below:

- 3000 motor units: 19.43°
- 4000 motor units: 37.98°
- 6000 motor units: 53.38°
- 7000 motor units: 54.04°

The results show that the arm exhibits progressive bending as the motor input increases. However, compared with the previous designs, the increase in bending angle becomes smaller for higher motor inputs, suggesting that the internal red wire structure introduces additional stiffness that limits the maximum achievable curvature of the arm.

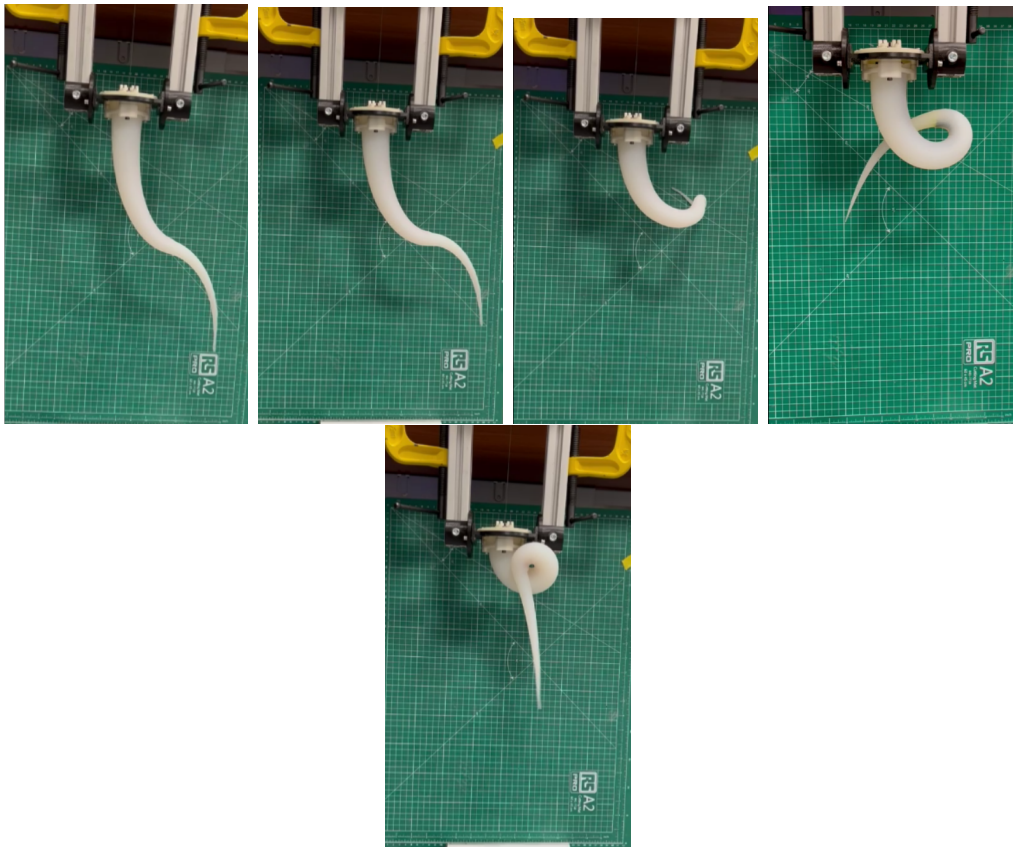

Figura 4.8: Deformation of the red-wire soft arm prototype under increasing motor actuation levels.

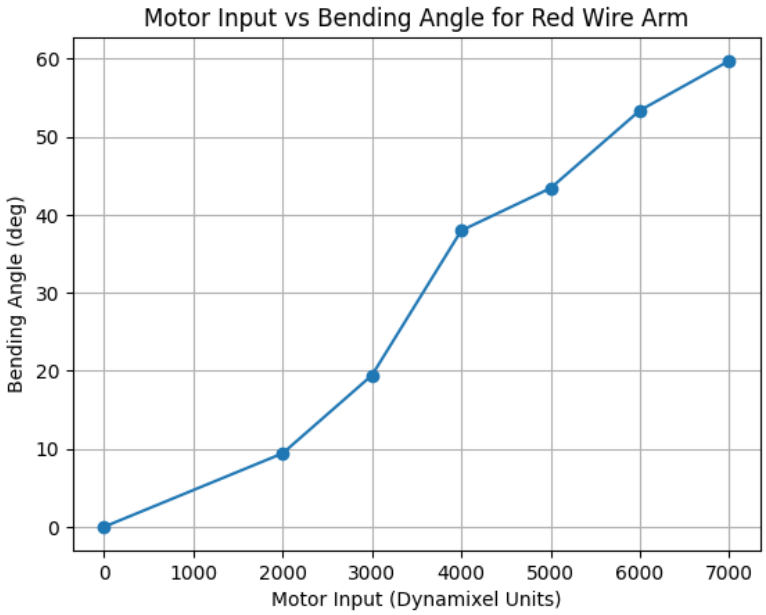

Figura 4.9: Relationship between the Dynamixel motor input and the resulting bending angle of the white-wire soft arm prototype.

4.4.4 Discussion of the Experimental Results

The experimental tests allowed the evaluation of the bending behaviour of the different soft robotic arm prototypes under tendon-driven actuation. By analysing the relationship between the motor input and the resulting bending angle, it was possible to investigate how the internal structural elements influence the mechanical response of the arm.

For all the tested configurations, the bending angle increases as the motor input increases. This behaviour confirms that the tendon-driven actuation mechanism successfully generates controlled deformation of the arm.

Despite this common behaviour, the experimental results highlight significant differences between the tested internal structures. In particular, the white-wire arm exhibited the largest bending angles, reaching approximately 74° at the highest motor input. This indicates that this configuration provides the highest level of compliance, allowing the silicone structure to deform more freely under tendon tension.

In contrast, the braided sleeve configuration showed a more moderate bending response. Although the bending angle increased with the motor input, the maximum curvature achieved was lower compared to the white-wire arm. The braided reinforcement likely constrains the radial deformation of the silicone body and

distributes the internal stresses more evenly, increasing the overall structural stiffness of the arm.

Similarly, the red-wire configuration exhibited a more limited bending behaviour compared to the white-wire prototype. The internal wires introduce additional stiffness along the arm structure, which restricts the deformation of the silicone body. As a consequence, the achievable curvature becomes more limited for higher actuation levels.

Another relevant observation concerns the nonlinear growth of the bending angle for higher motor inputs. In particular, the increase in curvature becomes progressively smaller at higher actuation values. This behaviour suggests the presence of mechanical constraints within the structure, such as material stiffness, geometric limitations, or tendon routing effects, which limit further deformation once a certain curvature is reached.

Overall, the results demonstrate that the internal structural elements play a fundamental role in determining the deformation capabilities of soft continuum arms. Different reinforcement strategies lead to different stiffness characteristics, which directly influence the relationship between tendon actuation and resulting curvature.

From a design perspective, these findings highlight how the mechanical response of soft robotic manipulators can be tuned by modifying the internal reinforcement structure. By selecting different internal elements, it is possible to adjust the balance between flexibility and structural stability depending on the desired manipulation capabilities.

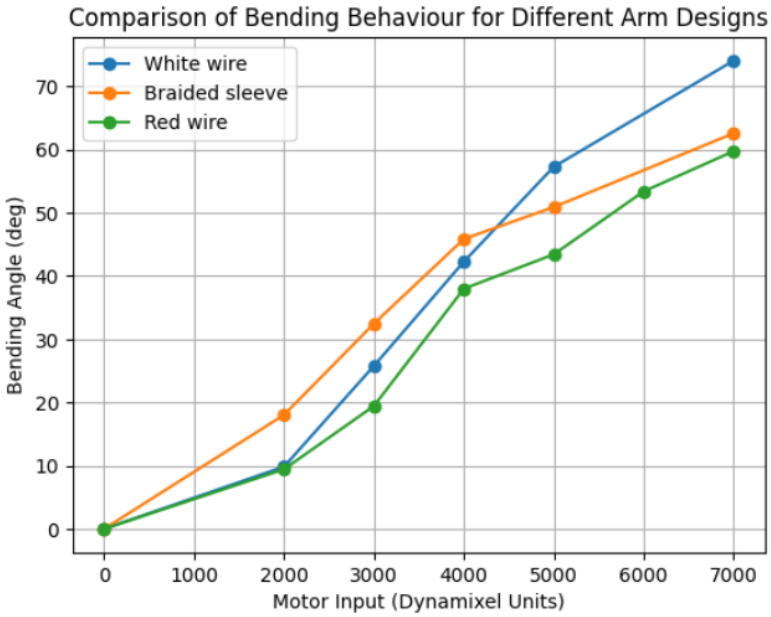

Figura 4.10: Relationship between the Dynamixel motor input and the resulting bending angle of the white-wire soft arm prototype.

Arm with Internal Skeleton

Although the previous configurations exhibit different bending behaviours, the differences in maximum curvature remain relatively limited in the final configurations. For this reason, an additional arm configuration incorporating an internal skeleton was investigated, in order to explore a more structurally distinct solution and assess its effect on bending performance.

To ensure a consistent and fair comparison with the previously tested configurations, the bending angle was evaluated over the same reference arm length. Specifically, the tracked point was placed at a distance of 277.13 mm from the base, corresponding to the reference length adopted for the other arm configurations. This approach enables a direct comparison of the bending behaviour across different designs, independently of their total length. As a consequence, the calculated bending angle does not include the final distal portion of the arm, where additional curling occurs.

The experimental results showed that this configuration required higher motor inputs to achieve comparable bending deformations. For a motor input of 7000 units, the measured bending angle was approximately 46.37°. By increasing the motor input to 9000 units, the bending angle increased up to approximately 98.91°.

So the results suggest that the internal skeleton increases the effective stiffness of the arm, requiring a larger actuation input to generate significant bending. At

the same time, the deformation pattern differs from the previous prototypes. In particular, the arm develops a more constrained curvature and, at higher actuation levels, a double-curling configuration can be observed.

This behaviour indicates that the internal skeleton does not only affect the magnitude of the bending angle, but also modifies the overall deformation mode of the structure. Rather than behaving as a homogeneous elastic body, the arm with internal skeleton exhibits a guided deformation influenced by the internal reinforcement.

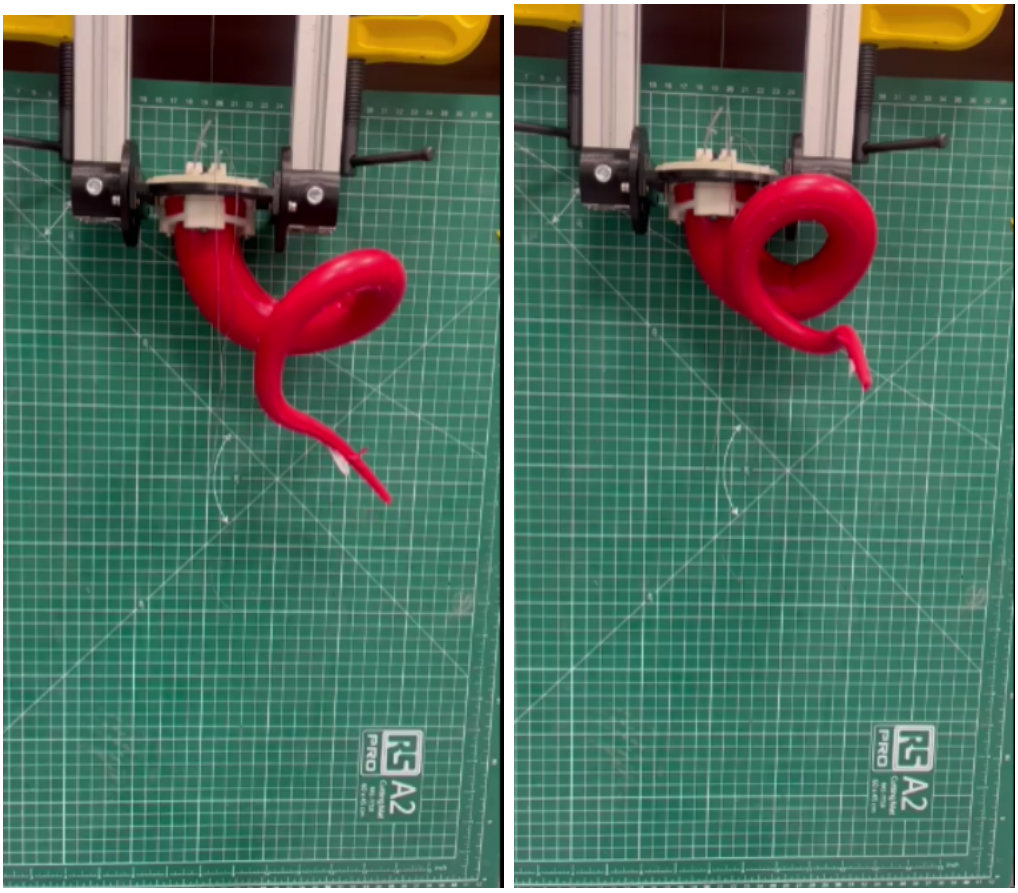

Figura 4.11: Deformation of the arm prototype with internal skeleton under different motor inputs. Left: configuration obtained with a motor input of 7000 units. Right: configuration obtained with a motor input of 11000 units, showing the development of a double-curling pattern.

4.5 Comparison of tip designs

A comparison between the configurations with and without internal skeleton highlights key differences in their mechanical response under tendon-driven actuation.

The arm without internal skeleton achieves a lower curvature for the same amount of tendon pulling, indicating a less effective transmission of the actuation input. In addition, this configuration exhibits a noticeable out-of-plane twisting, resulting in a less predictable and less controlled deformation. Furthermore, the bending is distributed along the entire length of the arm, leading to a less localized and less controllable motion.

On the other hand, the configuration incorporating the internal skeleton shows a higher curvature for the same tendon displacement, demonstrating a more efficient conversion of tendon input into bending. As observed in Fig. 4.12, the deformation is more localized near the distal region, while the rest of the arm remains relatively straight during the initial bending phase. Moreover, the presence of the internal skeleton suppresses undesired twisting and ensures a more stable and repeatable behaviour, maintaining the deformation within a well-defined plane. These observations highlight the role of the internal skeleton in enhancing bending efficiency, spatial localization of deformation, and overall stability, leading to a more controlled actuation response.

(a) Arm without internal skeleton.

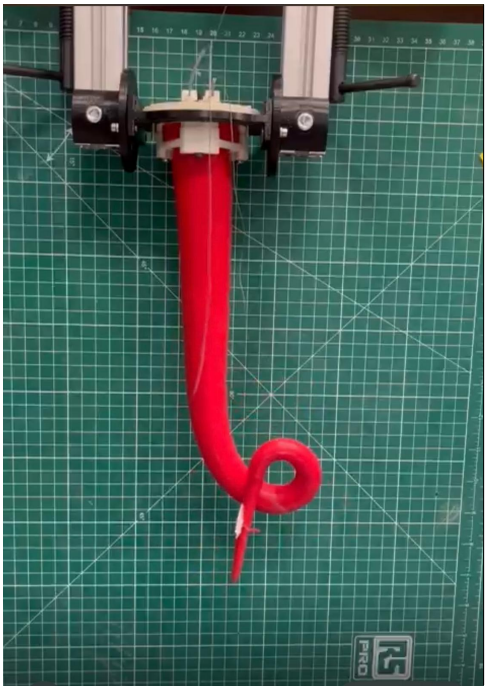

(b) Arm with internal skeleton.

Figura 4.12: Comparison of distal tip behaviour under tendon-driven actuation. The configuration without internal skeleton (a) achieves a larger curvature for the same tendon displacement, but exhibits significant out-of-plane twisting. In contrast, the arm with internal skeleton (b) shows reduced curvature due to increased stiffness, while ensuring a more stable and controlled deformation, with negligible twisting.

4.6 Mechanical Characterization of the Arm Tip

In addition to the bending experiments performed on the full arm prototypes, further tests were conducted to investigate the mechanical behaviour of the distal region of the arm. In particular, tensile tests were performed on arm configurations including the distal tip, in order to analyse the mechanical response of the tip under axial loading.

Experimental Setup

The experiments were carried out using a universal testing machine (Zwick/Roell). During the test, the base of the arm was rigidly fixed to the upper clamp of the machine. A controlled vertical displacement was applied, progressively stretching the arm while measuring the corresponding reaction force.

The machine recorded the applied force as a function of the imposed displacement, allowing the evaluation of the force–displacement behaviour of the tested arm tips.

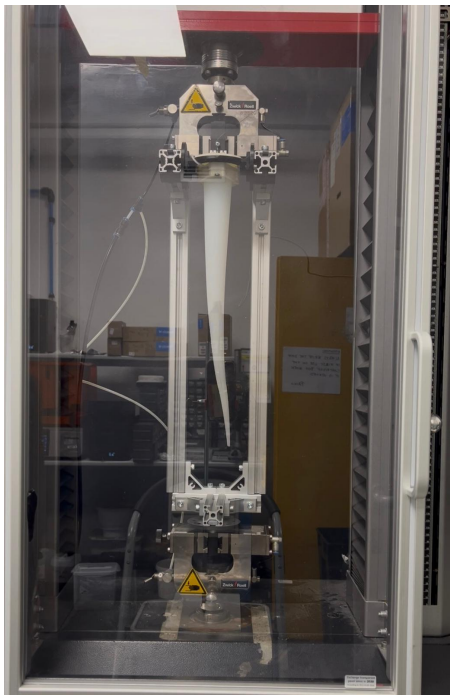

Figura 4.13: Experimental setup used for the tensile tests performed on the arm prototypes including the distal tip.

Tested Tip Configurations

Two different arm configurations were tested, including the distal tip.

The first configuration consisted of a homogeneous silicone arm reinforced with a fishing line and externally covered with a white cross-linked nylon thread. The total length of this prototype, including the tip, was about 31 cm.

The second configuration concerned the resin skeleton in the silicone body. The total length of this arm was about 47 cm, with a length of the internal skeleton of about 42 cm (33 cm excluding the distal tip and 42 cm including the tip).

Force–Displacement Results

For each configuration, multiple tensile tests were performed to evaluate the mechanical behaviour of the arm tip. The resulting force–displacement curves are reported in Figures 4.14 and 4.15.

These curves represent the measured reaction force as a function of the imposed displacement applied by the testing machine.

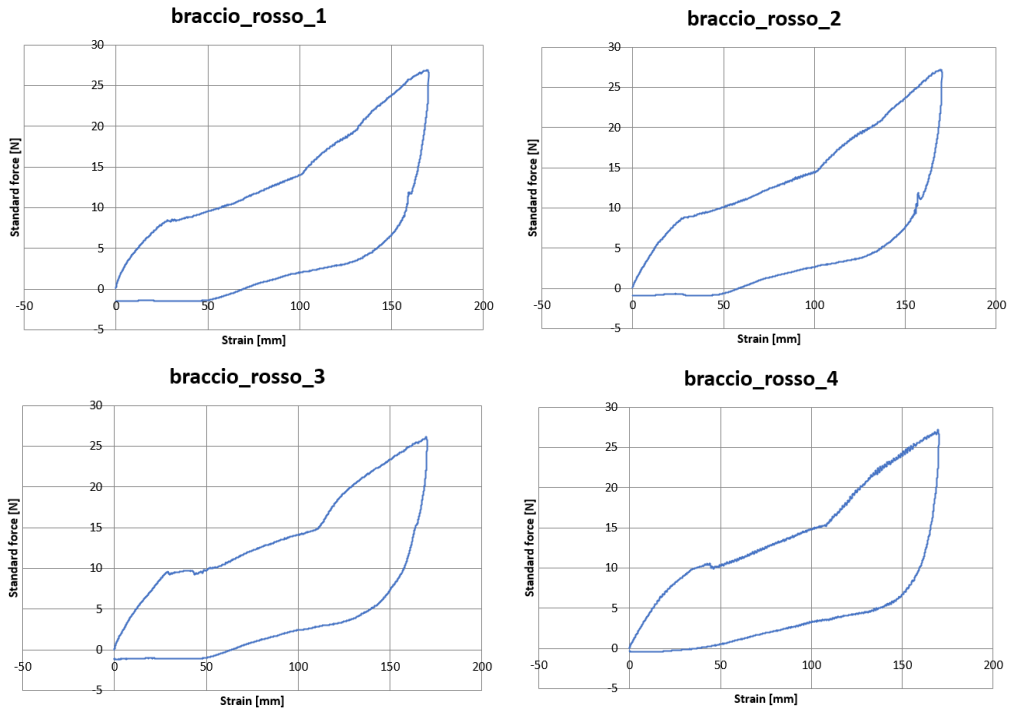

Figura 4.14: Force–displacement curves obtained for the arm configuration including the internal skeleton.

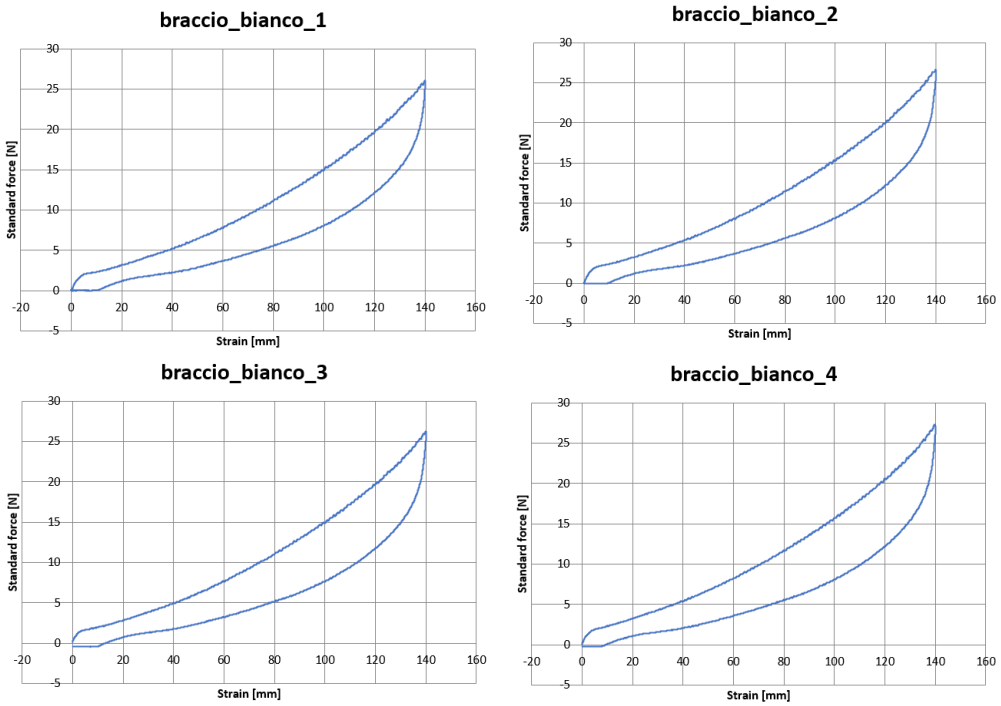

Figura 4.15: Force–displacement curves obtained for the silicone arm reinforced with fishing line and covered with white wire.

Comparison of Tip Behaviour

The comparison between the two configurations highlights clear differences in the mechanical behaviour of the arms with the tip.

The arm including the internal skeleton shows a higher resistance to deformation, as indicated by the larger forces required to reach similar displacement levels. This behaviour suggests that the internal skeleton significantly increases the effective stiffness of the distal region of the arm.

In contrast, the homogeneous silicone arm reinforced with the fishing line exhibits a more compliant mechanical response. Lower forces are required to achieve comparable displacements, indicating a more flexible structure where the deformation is mainly governed by the elastic behaviour of the silicone material.

Additionally, the force–displacement curves exhibit nonlinear behaviour and noticeable hysteresis between loading and unloading phases. This phenomenon is typical of soft elastomeric materials and reflects energy dissipation within the silicone structure.

Capitolo 5

Conclusion

Biological observations highlight that the distal tip of the octopus arm does not behave as a purely passive element, but plays an active role in exploration and interaction with the environment. In particular, the distal region exhibits continuous and fluid motion even in the absence of contact, suggesting an intrinsic dynamic behavior.

At the same time, the octopus demonstrates a high level of control along the entire arm. Although the arm can be considered mechanically continuous and structurally coherent along its length, the distal portion appears more flexible and responsive. This behavior is mainly related to its smaller size, which results in lower bending stiffness and a faster dynamic response. Therefore, the increased flexibility observed at the tip does not arise from a fundamentally different structure, but rather from a scaling effect along the arm.

Based on these observations, a series of robotic arms with different internal configurations was developed to investigate how such variations influence the overall mechanical behavior. This approach enabled a direct comparison between different design solutions and highlighted the role of internal architecture in determining the system response.

However, due to design and anchoring constraints, a small distal portion of the robotic arm remains made exclusively of silicone and is not directly actuated. As a result, the implemented tip does not fully replicate the continuous actuation observed in biological systems, representing a limitation of the current prototype.

Experimental tests with tendon-driven actuation showed a clear relationship between motor input and bending angle, confirming the system's ability to generate controlled curvature. The results demonstrate that both the type and the dimensions of the internal elements significantly affect the mechanical response of the arm.

Considering the global deformation (excluding the distal tip), the configuration with an internal skeleton achieves a larger curvature range, but requires greater tendon displacement and higher forces due to increased structural stiffness. In

contrast, the configuration with a braided nylon guide exhibits a more compliant response and smoother deformation.

When focusing on the distal region, a different trend emerges: the configuration with an internal skeleton enables greater, faster, and more controlled curvature, as well as improved localization of deformation. This behavior can be further interpreted by considering the effect of scale and the amount of material involved. In larger structures, characterized by a higher volume of silicone, the internal skeleton significantly increases overall stiffness, as both the material volume and the structural reinforcement contribute to resisting deformation. Consequently, higher forces and displacements are required to achieve comparable global curvature.

Conversely, in the distal region, characterized by smaller dimensions and reduced material volume, the stiffness introduced by the skeleton becomes less limiting and instead enhances control, allowing for more effective and localized bending..

Bibliography

[1] Daniela Rus e Michael T. Tolley. «Design, fabrication and control of soft robots». In: *Nature* 521.7553 (2015), pp. 467–475. DOI: 10.1038/nature14543 (cit. alle pp. 1, 2, 12).

[2] Cecilia Laschi, Barbara Mazzolai e Matteo Cianchetti. «Soft robotics: Technologies and systems pushing the boundaries of robot abilities». In: *Science Robotics* 1.1 (2016). DOI: 10.1126/scirobotics.aah3690 (cit. alle pp. 1, 5).

[3] George M. Whitesides. «Soft Robotics». In: *Angewandte Chemie International Edition* 57.16 (2018), pp. 4258–4273. DOI: 10.1002/anie.201800907 (cit. alle pp. 1, 4).

[4] Koichi Suzumori, Shigeru Iikura e Hiroyuki Tanaka. «Applying a Flexible Microactuator to Robotic Mechanisms». In: *IEEE Control Systems Magazine* 12.1 (1992), pp. 21–27. DOI: 10.1109/37.120449 (cit. a p. 2).

[5] William McMahan, Bryan A. Jones e Ian D. Walker. «Field Trials and Testing of the OctArm Continuum Manipulator». In: *Proceedings of the IEEE International Conference on Robotics and Automation (ICRA)*. 2006, pp. 2336–2341. DOI: 10.1109/ROBOT.2006.1642065 (cit. a p. 2).

[6] Eric Brown, Nicholas Rodenberg, John Amend, Ann Mozeika, Erik Steltz, Michael R. Zakin, Hod Lipson e Heinrich M. Jaeger. «Universal robotic gripper based on the jamming of granular material». In: *Proceedings of the National Academy of Sciences* 107.44 (2010), pp. 18809–18814. DOI: 10.1073/pnas.1003250107 (cit. a p. 2).

[7] Filip Ilievski, Aaron D. Mazzeo, Robert F. Shepherd, Xin Chen e George M. Whitesides. «Soft Robotics for Chemists». In: *Angewandte Chemie International Edition* 50.8 (2011), pp. 1890–1895. DOI: 10.1002/anie.201006464 (cit. a p. 2).

[8] Raphael Deimel e Oliver Brock. «A Novel Type of Compliant, Underactuated Robotic Hand for Dexterous Grasping». In: *Proceedings of Robotics: Science and Systems (RSS)*. 2014, pp. 1687–1692. DOI: 10.15607/RSS.2014.X.027 (cit. a p. 2).

[9] C. Laschi, B. Mazzolai e M. Cianchetti. «Soft robotics: Technologies and systems pushing the boundaries of robot abilities». In: *Advanced Robotics* 26.9 (2012), pp. 977–1000 (cit. alle pp. 2, 7, 32).

[10] Sarthak Sanan, Philip S. Lynn e Shane T. Griffith. «Pneumatic Torsional Actuators for Inflatable Robots». In: *Journal of Mechanisms and Robotics* 6.3 (2014), p. 031003. DOI: 10.1115/1.4027036 (cit. a p. 2).

[11] Andrew D. Marchese, Kristen Komorowski, Cagdas D. Onal e Daniela Rus. «Design and Control of a Soft and Continuously Deformable 2D Robotic Manipulation System». In: *Proceedings of the IEEE International Conference on Robotics and Automation (ICRA)*. 2014, pp. 2189–2196. DOI: 10.1109/ICRA.2014.6907161 (cit. a p. 2).

[12] Panagiotis Polygerinos, Zheng Wang, Kevin C. Galloway, Robert J. Wood e Conor J. Walsh. «Soft Robotic Glove for Combined Assistance and At-Home Rehabilitation». In: *Robotics and Autonomous Systems* 73 (2015), pp. 135–143. DOI: 10.1016/j.robot.2014.08.014 (cit. a p. 2).

[13] H. Lin, G. Leisk e B. Trimmer. «Soft Robots in Space: A Perspective for Soft Robotics». In: *Acta Futura* 6 (2013), pp. 69–79 (cit. a p. 3).

[14] Robert F. Shepherd, Filip Ilievski, Wonjae Choi, Stephen A. Morin, Adam A. Stokes, Aaron D. Mazzeo, Xin Chen, Michael Wang e George M. Whitesides. «Multigait Soft Robot». In: *Proceedings of the National Academy of Sciences* 108.51 (2011), pp. 20400–20403. DOI: 10.1073/pnas.1116564108 (cit. a p. 3).

[15] Stephen A. Morin, Robert F. Shepherd, Samuel W. Kwok, Adam A. Stokes, Alex Nemiroski e George M. Whitesides. «Camouflage and Display for Soft Machines». In: *Science* 337.6096 (2012), pp. 828–832. DOI: 10.1126/science.1222149 (cit. a p. 3).

[16] Michael T. Tolley, Robert F. Shepherd, Bobak Mosadegh, Kevin C. Galloway, Michael Wehner, Michael Karpelson, Robert J. Wood e George M. Whitesides. «A Resilient, Untethered Soft Robot». In: *Soft Robotics* 1.3 (2014), pp. 213–223. DOI: 10.1089/soro.2014.0008 (cit. a p. 3).

[17] Sangbae Seok, Cagdas D. Onal, Kyu-Jin Cho, Robert J. Wood, Daniela Rus e Sangbae Kim. «Meshworm: A Peristaltic Soft Robot with Antagonistic Nickel Titanium Coil Actuators». In: *IEEE/ASME Transactions on Mechatronics* 18.5 (2013), pp. 1485–1497. DOI: 10.1109/TMECH.2013.2250986 (cit. a p. 3).

[18] Erik Steltz, Ann Mozeika, Nicholas Rodenberg, Eric Brown e Heinrich M. Jaeger. «JSEL: Jamming Skin Enabled Locomotion». In: *Proceedings of the IEEE/RSJ International Conference on Intelligent Robots and Systems (IROS)*. 2009, pp. 5672–5677. DOI: 10.1109/IROS.2009.5354151 (cit. a p. 3).

[19] Cagdas D. Onal, Xin Chen, George M. Whitesides e Daniela Rus. «Soft Mobile Robots with On-Board Chemical Pressure Generation». In: *Proceedings of the International Symposium on Robotics Research (ISRR)*. 2011, pp. 1–16 (cit. a p. 3).

[20] Adam A. Stokes, Robert F. Shepherd, Stephen A. Morin, Filip Ilievski e George M. Whitesides. «A Hybrid Combining Hard and Soft Robots». In: *Soft Robotics* 1.1 (2014), pp. 70–74. DOI: 10.1089/soro.2013.0002 (cit. a p. 3).

[21] Cagdas D. Onal e Daniela Rus. «Autonomous Undulatory Serpentine Locomotion Utilizing Body Dynamics of a Fluidic Soft Robot». In: *Bioinspiration & Biomimetics* 8.2 (2013), p. 026003. DOI: 10.1088/1748-3182/8/2/026003 (cit. a p. 3).

[22] Michael T. Tolley, Robert F. Shepherd, Bobak Mosadegh, Kevin C. Galloway, Michael Wehner, Michael Karpelson, Robert J. Wood e George M. Whitesides. «An Untethered Jumping Soft Robot». In: *Proceedings of the IEEE/RSJ International Conference on Intelligent Robots and Systems (IROS)*. 2014, pp. 561–566. DOI: 10.1109/IROS.2014.6942593 (cit. a p. 3).

[23] Koichi Suzumori, Satoshi Endo, Takashi Kanda, Nobuhiro Kato e Hiroyuki Suzuki. «A Bending Pneumatic Rubber Actuator Realizing Soft-Bodied Manta Swimming Robot». In: *Proceedings of the IEEE International Conference on Robotics and Automation (ICRA)*. 2007, pp. 4975–4980. DOI: 10.1109/ROBOT.2007.364246 (cit. a p. 3).

[24] Andrew D. Marchese, Cagdas D. Onal e Daniela Rus. «Autonomous Soft Robotic Fish Capable of Escape Maneuvers Using Fluidic Elastomer Actuators». In: *Soft Robotics* 1.1 (2014), pp. 75–87. DOI: 10.1089/soro.2013.0009 (cit. a p. 3).

[25] Rolf Pfeifer, Max Lungarella e Fumiya Iida. «The Challenges Ahead for Bio-Inspired "Soft" Robotics». In: *Communications of the ACM* 55.11 (2012), pp. 76–87. DOI: 10.1145/2366316.2366335 (cit. a p. 4).

[26] Sangbae Kim, Cecilia Laschi e Barry Trimmer. «Soft robotics: a bioinspired evolution in robotics». In: *Trends in Biotechnology* 31.5 (2013), pp. 287–294. DOI: 10.1016/j.tibtech.2013.03.002 (cit. alle pp. 4, 7).

[27] Gianmarco Mengaldo, Federico Renda, Steven L. Brunton, Moritz Bächer, Marcello Calisti, Christian Duriez, Gregory S. Chirikjian e Cecilia Laschi. «A concise guide to modelling the physics of embodied intelligence in soft robotics». In: *Nature Reviews Physics* 4.9 (2022), pp. 595–613. DOI: 10.1038/s42254-022-00481-z (cit. a p. 4).

[28] Oncay Yasa, Yasunori Toshimitsu, Mike Y. Michelis, Lewis S. Jones, Miriam Filippi, Thomas Buchner e Robert K. Katzschmann. «An Overview of Soft Robotics». In: *Annual Review of Control, Robotics, and Autonomous Systems* 6 (2023), pp. 1–29. DOI: 10.1146/annurev-control-062322-100607 (cit. a p. 5).

[29] Ouriel Bliah, Chidanand Hegde, Joel Ming Rui Tan e Shlomo Magdassi. «Fabrication of Soft Robotics by Additive Manufacturing: From Materials to Applications». In: *Chemical Reviews* 125 (2025), pp. 7275–7320. DOI: 10.1021/acs.chemrev.4c00749 (cit. a p. 5).

[30] William M. Kier e Kevin K. Smith. «Tongues, tentacles and trunks: the biomechanics of movement in muscular-hydrostats». In: *Zoological Journal of the Linnean Society* 83.4 (1985), pp. 307–324 (cit. alle pp. 6, 7, 9–11).

[31] William M. Kier e Kevin K. Smith. «Muscles, skeletons, and movement». In: *American Zoologist* 31.3 (1991), pp. 524–538 (cit. alle pp. 6, 9).

[32] William M. Kier. «The diversity of hydrostatic skeletons». In: *Journal of Experimental Biology* 205.6 (2002), pp. 933–945 (cit. alle pp. 7, 11).

[33] Pietro P. C. Graziadei. «The nervous system of the arms of the octopus». In: *Zeitschrift für Zellforschung und mikroskopische Anatomie* 114 (1971), pp. 1–23 (cit. a p. 7).

[34] Leonardo Margheri, Giovanna Ponte, Barbara Mazzolai e Cecilia Laschi. «Ultrasound imaging of octopus arm muscles». In: *Journal of Experimental Biology* 214.22 (2011), pp. 3727–3736 (cit. a p. 8).

[35] Sara Fossati, Fabio Benfenati e Lucia Zullo. «Morphological characterization of the Octopus vulgaris arm». In: *Vie et Milieu – Life and Environment* 61.4 (2011), pp. 193–200 (cit. alle pp. 8, 9).

[36] Barbara Mazzolai, Leonardo Margheri e Cecilia Laschi. «Measurements of octopus arm elongation». In: *Journal of Experimental Biology* 216.19 (2013), pp. 3727–3736 (cit. alle pp. 10, 11).

[37] Barbara Mazzolai e Cecilia Laschi. «Soft-Robotic Arm Inspired by the Octopus». In: *Bioinspiration & Biomimetics* 10.3 (2015), p. 035005. DOI: 10.1088/1748-3190/10/3/035005 (cit. a p. 12).

[38] Matteo Cianchetti, Andrea Arienti, Maurizio Follador, Barbara Mazzolai, Paolo Dario e Cecilia Laschi. «Design concept and validation of a robotic arm inspired by the octopus». In: *Materials Science and Engineering C* 31 (2011), pp. 1230–1239 (cit. a p. 12).

[39] Panagiotis Polygerinos, Nikolaus Correll, Samuel A. Morin et al. «Soft Robotics: Review of Fluid-Driven Intrinsically Soft Devices; Manufacturing, Sensing, Control, and Applications in Human–Robot Interaction». In: *Advanced Engineering Materials* 19.12 (2017), p. 1700016. DOI: 10.1002/adem.201700016 (cit. a p. 12).

[40] Cecilia Laschi, Matteo Cianchetti, Barbara Mazzolai, Lorenzo Margheri, Marco Follador e Paolo Dario. «A Soft Robot Arm Inspired by the Octopus». In: *Advanced Robotics* 26.7 (2009), pp. 709–727. DOI: 10.1163/156855309X12550713012445 (cit. a p. 12).

[41] Barbara Mazzolai, Laura Margheri, Matteo Cianchetti, Paolo Dario e Cecilia Laschi. «Soft-robotic arm inspired by the octopus: II. From artificial requirements to innovative technological solutions». In: *Bioinspiration & Biomimetics* 7.2 (2012), p. 025005. DOI: 10.1088/1748-3182/7/2/025005 (cit. alle pp. 13, 14, 16).

[42] Michele Giorelli, Federico Renda, Marcello Calisti, Alberto Arienti, Gianni Ferri e Cecilia Laschi. «A two-dimensional inverse kinetics model of a cable-driven manipulator inspired by the octopus arm». In: *Bioinspiration & Biomimetics* 7.2 (2012), p. 025006. DOI: 10.1088/1748-3182/7/2/025006 (cit. a p. 13).

[43] M. Calisti, F. Corucci, C. Laschi e P. Dario. «An octopus-bioinspired solution to movement and manipulation for soft robots». In: *Bioinspiration & Biomimetics* 6.3 (2011), p. 036002 (cit. alle pp. 13, 14, 16, 32).

[44] P. Rao, Q. Peyron, S. Lilge e J. Burgner-Kahrs. «How to Model Tendon-Driven Continuum Robots and Benchmark Modelling Performance». In: *Frontiers in Robotics and AI* 7 (2021), p. 630245. DOI: 10.3389/frobt.2020.630245 (cit. a p. 14).

[45] Robert J. Webster e Bryan A. Jones. «Design and Kinematic Modeling of Constant Curvature Continuum Robots: A Review». In: *The International Journal of Robotics Research* 29.13 (2010), pp. 1661–1683. DOI: 10.1177/0278364910368147 (cit. a p. 14).

[46] I. D. Walker et al. «Continuum robot arms inspired by cephalopods». In: *International Journal of Robotics Research* 25.5–6 (2006), pp. 427–440 (cit. a p. 32).

[47] Bertrand Tondu. «Modelling of the McKibben artificial muscle: A review». In: *Journal of Intelligent Material Systems and Structures* 23.3 (2012), pp. 225–253. DOI: 10.1177/1045389X11435435 (cit. a p. 35).

[48] Yasmin Ansari, Mariangela Manti, Egidio Falotico, Yoan Mollard, Matteo Cianchetti e Cecilia Laschi. «Towards the development of a soft manipulator as an assistive robot for personal care of elderly people». In: *International Journal of Advanced Robotic Systems* 14 (2017), pp. 1–17. DOI: 10.1177/1729881416687132 (cit. a p. 43).

[49] Zhanchi Wang, Nikolaos M. Freris e Xi Wei. «SpiRobs: Logarithmic spiral-shaped robots for versatile grasping across scales». In: *Device* 3 (2025). Open Access, p. 100646. DOI: 10.1016/j.device.2024.100646. URL: https://doi.org/10.1016/j.device.2024.100646 (cit. alle pp. 51, 52, 54).

[50] M. Cianchetti, T. Ranzani, G. Gerboni, T. Nanayakkara, K. Althoefer, P. Dasgupta e A. Menciassi. «Soft robotics technologies to address shortcomings in today's minimally invasive surgery». In: *IEEE Robotics & Automation Magazine* 21.3 (2014), pp. 10–21.

[51] T. Ranzani, M. Cianchetti, G. Gerboni, I. De Falco e A. Menciassi. «A soft modular manipulator for minimally invasive surgery: Design and characterization of a single module». In: *Soft Robotics* 3.2 (2016), pp. 72–85.

[52] D. Rus e M. T. Tolley. «Design, fabrication and control of soft robots». In: *Nature* 521 (2015), pp. 467–475.

[53] C. Laschi e M. Cianchetti. «Soft robotics: New perspectives for robot bodyware and control». In: *Soft Robotics* 1.1 (2014), pp. 3–16.